[AMERICAN JOURNAL OF SCIENCE, VOL. 310, NOVEMBER, 2010, P. 1054–1080, DOI 10.2475/09.2010.11]

U-Pb GEOCHRONOLOGY AND GEOCHEMISTRY OF THE DASHIBAO BASALTS IN THE SONGPAN-GANZI TERRANE, SW CHINA, WITH IMPLICATIONS FOR THE AGE OF EMEISHAN VOLCANISM

JIAN-WEI ZI*,**, WEI-MING FAN*, YUE-JUN WANG*, PETER A. CAWOOD**,§, TOU-PING PENG*, LIN-HUA SUN*, and ZHEN-QIANG XU***

ABSTRACT. Permian marine basalts (the Dashibao Formation) in the Songpan-Ganzi Terrane to the west of the Yangtze Block, SW China, yield a SHRIMP zircon U-Pb weighted mean age of 263 ± 2 Ma. The Dashibao basalts are characterized by high TiO_2 contents (1.73-4.65 wt. %) and Ti/Y ratios with a mean of 577, and OIB-like rare earth element (REE) and incompatible element patterns. Geochemical variation within the basalt succession allows division into two groups; Group 1 with an alkaline composition is distinguished by higher TiO_2 and P_2O_5 contents, along with higher Ti/Y and Sm/Yb ratios than the underlying Group 2 that consists predominantly of tholeiitic lavas. Both groups possess weakly to moderately positive $\varepsilon_{Nd}(t)$ values (0.82 to 5.28), but the Group 2 tholeiitic basalts show relatively depleted signatures (most $\varepsilon_{Nd}(t) > 2.5$) when compared to their Group 1 counterparts ($\varepsilon_{Nd}(t) < 2.5$). REE modeling is consistent with variable degrees of melting of primitive mantle within the garnet stability field, and reveals that the Group 1 alkaline basalts could have been generated by lower degrees of melting (5-11%) than the Group 2 tholeiites (up to 19%). The initial Nd isotope discrepancy is interpreted in terms of depleted asthenospheric involvement in the early stage Group 2 tholeiitic magma. Combined geochronology, petrography and geochemistry for the Dashibao Formation confirms that it was temporally and genetically associated with the Emeishan basalts, and is therefore an integral part of the Emeishan large igneous province. The new zircon U-Pb dating supports the view that the Emeishan volcanism could be a boundary event occurring at or around the Middle-Late Permian (the Guadalupian-Lopingian) transition, and thereby confirms the validity of a causal connection with the end-Guadalupian mass extinction.

INTRODUCTION

The Emeishan large igneous province (LIP) of southwestern China includes voluminous high- and low-Ti basalts, ore-bearing mafic-ultramafic intrusions and associated alkaline and felsic rocks (Song and others, 2001; Xu and others, 2001; Zhang and Wang, 2002; Xiao and others, 2004; Zhong and others, 2007; Zhou and others, 2008), and has a stratigraphically well-constrained emplacement age of late Middle Permian with a short eruption duration (<2 Ma, Huang and Opdyke, 1998; Ali and others, 2005). Although challenged by some recent work (Peate and Bryan, 2008), a mantle plume-induced mechanism for the formation of this large igneous province has been well documented and widely accepted (Chung and Jahn, 1995; Xu and others, 2004).

The denudation pattern of the Maokou Formation, which directly underlies the Emeishan LIP, indicates that the Emeishan basalts have a roughly circular distribution. Such a feature can be best explained if a mantle plume invoked up-doming prior to the eruption of the basalts (He and others, 2003; He and others, 2006). This enables recognition of Inner (highly uplifted), Intermediate and Outer (negligibly uplifted)

* Key Laboratory of Isotope Geochronology and Geochemistry, Guangzhou Institute of Geochemistry, Chinese Academy of Sciences, 511 Kehua Street, Guangzhou 510640, China
** School of Earth and Environment, University of Western Australia, 35 Stirling Highway Crawley, WA, 6009 Australia; Jianwei Zi Email: zijw@cyllene.uwa.edu.au
*** China Geological Survey, 45 Fuwai Street, Beijing 100037, China
§ Now at: Department of Earth Sciences, Irvine Building, University of St. Andrews, North Street, St. Andrews, KY16 9AL, Fife, Scotland, United Kingdom; pac20@st-andrews.ac.uk

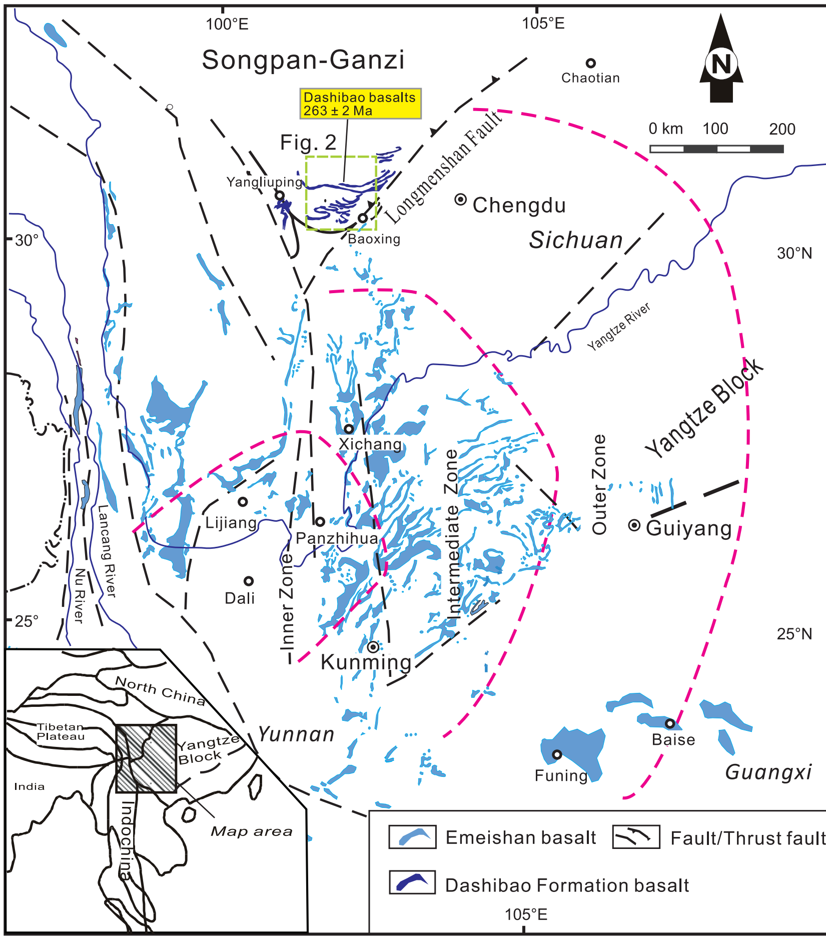

Fig. 1. Schematic map showing the distribution of the Permian flood basalts and the Inner, Intermediate and Outer zones of the Emeishan large igneous province (modified after He and others, 2003).

zones with igneous activity focused in the center of the province (Inner and Intermediate zones), although exposure of the basaltic rocks associated with the Emeishan LIP event is relatively poor in the Outer Zone (fig. 1). Fan and others (2008) recently reported a set of marine basalts from the Baise area in western Guangxi Province (corresponding to the Outer Zone, see fig. 1 for location), with age and geochemistry comparable to those of the Emeishan basalts, and proposed that these basalts constitute part of the Emeishan LIP. Abundant exposures of marine basalts also occur in the Songpan-Ganzi Terrane and adjacent areas (for example, Yidun terrane, Song and others, 2004), northwestern Sichuan Province, which are separated from those on the western Yangtze Block by the Longmenshan fault zone, and have been mapped as the Dashibao Formation (SBGMR, 1991, 1997). Although the issue of their relationship to the Emeishan LIP has been addressed in some recent publications (Xiao and Xu, 2005; Song and others, 2006), the Dashibao basalts, especially their eruption age, remain poorly documented. Moreover, Emeishan flood volcanism has been linked to the end-Guadalupian mass extinction (Middle-Late Permian boundary) (Chung and others, 1998; Ali and others, 2002; Zhou and others, 2002; Wignall and others, 2009). It is thus crucial to accurately constrain the eruption age, duration and extent of the LIP. However, an accurate temporal framework for the province remains to be firmly established.

In this paper, we present the results of a combined SHRIMP zircon U-Pb geochronological and geochemical study, including Sr-Nd isotope data on the Dashibao basalts, to determine their age and petrogenesis. Paleogeographic reconstructions at the time of eruption of the LIP suggest thinned lithosphere below the Dashibao Formation relative to the central zone of the LIP and we investigate the implication of this in understanding spatial and temporal trends in the province. The new zircon U-Pb age for the Dashibao basalts also places important constraints on Emeishan volcanism that, in combination with available radiometric age data from other components of the LIP, has great significance for establishing an accurate temporal framework for this important late Paleozoic igneous event.

GEOLOGICAL SETTING AND PETROLOGY

The Emeishan LIP is situated in the western part of the Yangtze Block (fig. 1). Biostratigraphic and sedimentologic data indicate that this region underwent rapid uplift at the end of the late Paleozoic, which is considered to be related to the impact of a mantle plume with the Yangtze lithosphere (He and others, 2003; Xu and others, 2004; He and others, 2006). The Emeishan LIP was disrupted and deformed in the Mesozoic and Cenozoic by post-emplacement faulting associated with the development of the Songpan-Ganzi Terrane and the Indo-Eurasian collision (Chung and Jahn, 1995 and references therein). Due to later disruption and erosion, the original size of the province is difficult to estimate, but its main outcrops cover an area of ~250,000 km^2 and constitute the largest geologic feature in SW China. The province consists of flood basalts, spatially associated felsic to mafic-ultramafic intrusions, some of which host giant Fe-Ti-V oxide deposits (Zhou and others, 2005). The volcanic succession is unconformably sandwiched between the underlying Middle Permian Maokou Formation (limestone) and the overlying Late Permian Xuanwei Formation (sandstone and mudstone). The lava piles range from several hundred meters up to 5 km in thickness (Chung and Jahn, 1995; Xu and others, 2001; Zhou and others, 2005). They are composed predominantly of basaltic lavas and pyroclastics, with minor amounts of picrites, basaltic andesites and alkaline rocks. The Emeishan basalts can be divided primarily on the basis of TiO_2 content and Ti/Y ratio into a low-Ti series, which occupies stratigraphically lower levels, and a high-Ti series, which dominates in the upper part of the volcanic succession. A mantle-plume model is invoked to explain the geological features such as the voluminous flood basalts, ultramafic lavas, short-duration, regional crustal doming and lower crustal seismic velocity layers (Chung and others, 1998; He and others, 2003; Xu and others, 2004; Xu and He, 2007).

The basalts of the Dashibao Formation lie beyond the Yangtze Block, within the Songpan-Ganzi Terrane, SW China, along the northeastern margin of the Tibetan Plateau (fig. 1). The terrane is separated from the Yangtze Block by the Longmenshan thrust belt (Burchfiel and others, 1995; Chen and Wilson, 1996). Neoproterozoic to late Paleozoic strata in the terrane and the Yangtze Block are similar and they are considered to have been contiguous until the Permian, when extension resulted in formation of an ocean basin around a mid-ocean ridge triple junction, which acted as a major sink for Triassic sediments derived from erosion of the Dabie-Sulu orogenic belt to the northeast (Chang, 2000; Yin and Harrison, 2000).

The Dashibao Formation occurs within a sequence composed of Proterozoic basement, Ordovician to Silurian strata, Devonian to Lower Permian limestones and Triassic clastic rocks (fig. 2). The formation crops out in a 400 km long belt in western Sichuan Province, and its exposure is apparently controlled by the Longmenshan Thrust Fault and the arcuate tectonic belt along the southeastern margin of the

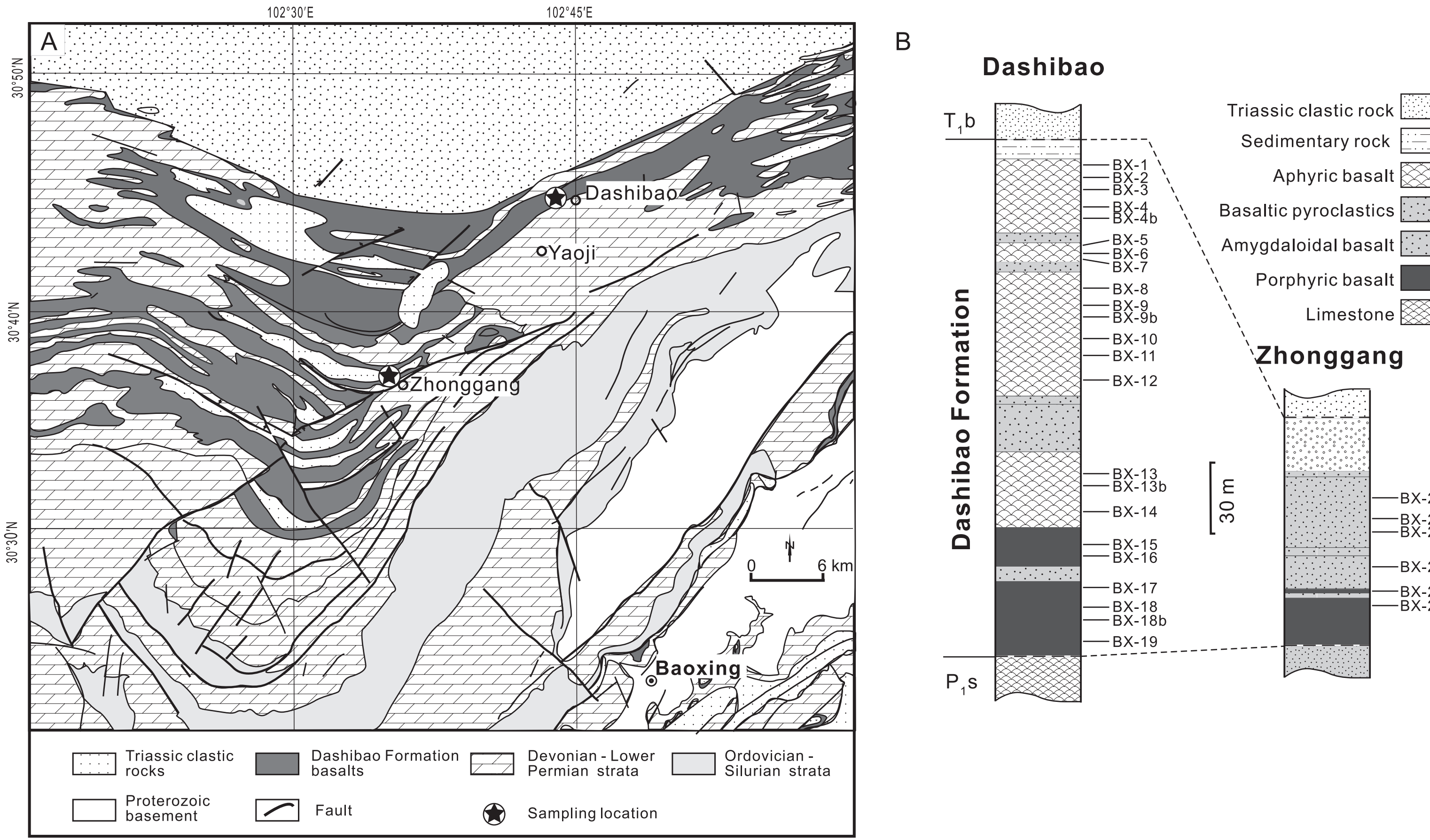

Fig. 2. (A) Simplified geological map of the Baoxing area in western Sichuan Province emphasizing the distribution of the Dashibao Formation basalts (after SBGMR, 1976, 1983). (B) Composite stratigraphic sections through the Dashibao Formation at Dashibao and Zhonggang showing position of samples. P_1s, Lower Permian Sandaoqiao Formation (limestone); T_1b, Lower Triassic Bocigou Formation (clastic rocks).

Songpan-Ganzi Terrane (figs. 1 and 2A). The basalts of the formation show pillow structures, indicative of a submarine environment, and consist of multiple flows with flow tops marked by pyroclastics and thin sedimentary intercalations (fig. 2B). The main basalt pile ranges in thickness from tens of meters to around 2500 m.

The studied samples were collected from the Dashibao and Zhonggang sections (fig. 2) in Baoxing County. The 215 m thick Dashibao section consists predominantly of fine-grained massive basalts, porphyritic basalts and basaltic pyroclastic rocks, and lies unconformably on the Sandaoqiao Formation (dark gray brecciated limestone containing late Early Permian fusulinid fossils, including *Neoschwagerlna sp.* and *Verbeekina sp.*), which is equivalent to the Maokou Fomation limestone of the western Yangtze Block. The lava sequence is covered by uppermost Permian sedimentary rocks, which are overlain conformably by lower Triassic clastic strata. The entire sequence underwent lower greenschist facies metamorphism in the Mesozoic (Huang and others, 2003). The basalt samples contain variable proportions of clinopyroxene (10-15 modal %), plagioclase (5-15 modal %) and olivine (3-5 modal %) phenocrysts set in a fine-grained to aphanitic groundmass composed of plagioclase, clinopyroxene and minor apatite and opaque oxides. Metamorphism of the samples is represented by alteration of plagioclase to albite and some chloritization of groundmass and ferromagnesium mineral phases.

SAMPLE PREPARATION AND ANALYTICAL METHODS

Zircons for geochronology were separated by conventional heavy liquid and magnetic techniques, then handpicked under a binocular microscope, and mounted in epoxy. The mount was polished to expose the center of the grains and coated with gold. The grains were photographed optically using transmitted and reflected light, and cathodoluminescence (CL) images were obtained on a scanning electron microscope and were used to select the initial analytical sites. U-Pb isotopic ratios were measured on the sensitive high-resolution ion microprobe (SHRIMP II) at the Beijing SHRIMP Center, the Chinese Academy of Geological Sciences. Detailed analytical procedures follow Song and others (2002). Quoted ages are $^{206}Pb/^{238}U$ ages and are based on the assumption that the bias in the measured $^{206}Pb/^{238}U^+$ ratio can be described by the same power law relationship between $^{206}Pb/^{238}U^+$ and UO^+/U^+ for the analytical standard and samples (Williams, 1998). SL13 (with an age of 572 Ma and U content of 238 ppm) and TEMORA (with an age of 417 Ma) (Black and others, 2003), were used as the calibration standards. The common lead correction was applied using the measured ^{204}Pb value (Compston and others, 1984). Errors for individual analyses are at the 1 σ level, and weighted mean ages are quoted with 95 percent confidence limits. Data processing was carried out using the Isoplot and Squid programs of Ludwig (2001a, 2001b).

For whole-rock geochemical studies, samples were crushed to 200-mesh using an agate mill. Major elements were determined by X-ray fluorescence spectrometry at the Hubei Institute of Geology and Mineral Resources, the Chinese Ministry of Land and Resources. Trace element analyses were performed at the Institute of Geochemistry, the Chinese Academy of Sciences (CAS) by inductively coupled plasma mass spectrometry (ICP-MS). About 100 mg samples were digested with 1 ml of HF and 0.5 ml HNO_3 in screw top PTFE-lines stainless steel bombs at 190°C for 12 hours. Detailed sample preparation methodology and analytical procedure followed Qi and others (2000). Reproducibility is better than 95 percent and the analytical error is less than 5 percent for elements $>$10ppm, less than 8 percent for those $<$10ppm, and about 10 percent for transition metals based on repetitive analyses of BHV-1 and AMH-1 standards.

Analyses of Sr and Nd isotopic ratios were performed by multi-collector inductively coupled plasma mass spectrometry (MC-ICP-MS) at the Guangzhou Institute of Geochemistry, CAS. Sample preparation and chemical separation followed Liang and others (2003). The total procedure blanks were $<5 \times 10^{-10}$g for Sr and $<5\times10^{-11}$g for Nd. The mass fractionation corrections for isotopic ratios are based on $^{86}Sr/^{88}Sr$ = 0.1194 and $^{146}Nd/^{144}Nd$ = 0.7219, respectively. The measured $^{87}Sr/^{86}Sr$ ratio of the NBS987 standard and $^{143}Nd/^{144}Nd$ ratio of the La Jolla standard were 0.710265 ± 12 (2σ) and 0.511862 ± 10 (2σ), respectively. $^{87}Rb/^{86}Sr$ and $^{147}Sm/^{144}Nd$ ratios were calculated using the Rb, Sr, Sm and Nd abundances measured by ICP-MS.

ANALYTICAL RESULTS

SHRIMP Zircon U-Pb Geochronology

The analyzed sample is a massive porphyric basalt from Dashibao [BX-18b, (E102°44.9′, N30°44.2′)] in northwestern Sichuan Province (fig. 2). Analytical results for zircons are presented in table 1, and a cathodoluminescence image of representative zircons is shown in figure 3A. The zircons are subhedral, transparent to light brown, and are prismatic in shape with length to width ratios of 2–3:1, and they exhibit a similar internal morphology with planar oscillatory zoning (fig. 3A). Sixteen analyses on sixteen grains show a range of Th (331-1321 ppm) and U (386-801ppm) contents with relatively high Th/U ratios (0.86-1.68) (table 1; see also fig. 3B), indicative of an igneous origin. These analyses form a single population on the concordia plot and give a weighted mean $^{206}Pb/^{238}U$ age of 263 ± 2 Ma with a MSWD value of 0.48 (fig. 3C). This age is considered to represent the crystallization age of the magmatic zircons, and is interpreted as the best estimation of the formation age for the Dashibao Formation basalts.

Geochemical Characteristics

Elemental data for the Dashibao Formation basalts are listed in table 2. Consistent with petrographic observation, the samples display alteration features, as reflected by high loss on ignition (LOI) ranging from 2.12 up to 7.86. They exhibit variations in major oxide compositions, for example: SiO_2 = 45.05 to 54.39 weight percent (recalculated volatile-free to 100%), TiO_2 = 1.79 to 4.92 weight percent, Fe_2O_3 = 11.67 to 17.07 weight percent, MgO = 4.47 to 7.80 weight percent (*mg*# = 0.42 to 0.57), and total alkalis ($Na_2O + K_2O$) = 2.63 to 6.01 weight percent. Chromium and Ni contents vary from 31 to 193 ppm and 21 to 106 ppm, respectively.

Geochemical variation within the Dashibao basalts with respect to TiO_2, Ti/Y and P_2O_5 allow division into two groups (table 2). Group 1 basalts generally possess higher Ti (TiO_2 >2.5 wt. %, Ti/Y >550) and P_2O_5 (mean 0.35 wt. %) contents than the Group 2 basalts (TiO_2 <2.5 wt. %, most Ti/Y <550 and mean P_2O_5 = 0.25 wt. %). K_2O and/or Na_2O contents of some high-LOI samples show significant deviation due to alteration (table 2), hence SiO_2 vs. Nb/Y (fig. 4A) rather than K_2O+Na_2O vs. SiO_2 is used to discriminate the samples. In figure 4A, analyses of groups 1 and 2 plot in the fields of alkaline and sub-alkaline basalts, respectively, although some Group 2 basalts do plot in the alkaline field. On Ti-Zr-Y and Nb-Zr-Y discrimination diagrams (figs. 4B and 4C), the Dashibao basalts mostly fall in the within-plate field with Group 1 in the alkali basalt and the majority of Group 2 data in the combined field of tholeiite and alkali basalt. On Harker variation diagrams (fig. 5), the two groups are effectively separated on plots of TiO_2 and P_2O_5 versus SiO_2. Group 2 samples show negative correlations between SiO_2 and Fe_2O_3, CaO, Al_2O_3 and MnO. No coherent trend is observed among other oxides for either group. Chromium and Ni show weakly positive correlation with *mg*# for Group 2 (figs. 6A and 6B), whereas all of the immobile trace elements (for example, Zr, REE, Th and Ta) have a positive correlation with Nb contents for both groups (figs. 6C-F).

Chondrite-normalized REE patterns of the basalts show LREE enrichment (figs. 7A and 7B), subparallel to that of ocean island basalt (OIB), and also similar to those of

TABLE 1

SHRIMP zircon U-Pb dating results for the Dashibao basalt (sample BX-18b) from the Songpan-Ganzi Terrane, SW China

Spot	Concentration (ppm)			Th/U	^{204}Pb Corrected ratio								Calculated apparent age (Ma)					
	U	Th	Pb		^{206}Pb/^{238}U	%err	^{208}Pb/^{232}Th	%err	^{207}Pb/^{206}Pb	%err	^{207}Pb/^{235}U	%err	^{207}Pb/^{206}U	1σ err	^{208}Pb/^{232}Th	1σ err	^{206}Pb/^{238}U	1σ err
1.1	665	894	24	1.34	0.0411	1.8	0.0132	2.1	0.05163	2.5	0.29	3.1	269	57	265	6	260	5
2.1	695	687	25	0.99	0.0417	1.8	0.0131	2.2	0.05224	2.1	0.30	2.8	296	48	262	6	263	5
3.1	801	1321	29	1.65	0.0417	1.8	0.0129	2.0	0.04959	2.0	0.29	2.7	176	46	259	5	264	5
4.1	386	331	14	0.86	0.0421	1.9	0.0124	3.3	0.04659	4.9	0.27	5.2	28	117	249	8	266	5
5.1	754	1014	27	1.34	0.0413	1.9	0.0125	2.4	0.04930	2.8	0.28	3.4	162	66	251	6	261	5
6.1	644	749	23	1.16	0.0418	2.0	0.0128	3.6	0.05073	8	0.29	8.3	229	186	256	9	264	5
7.1	694	749	26	1.08	0.0425	1.8	0.0132	2.4	0.04951	3.9	0.29	4.3	172	91	265	6	268	5
8.1	664	1115	24	1.68	0.0416	1.8	0.0130	2.1	0.05059	2.3	0.29	2.9	222	53	260	6	263	5
9.1	541	646	20	1.19	0.0417	1.9	0.0123	2.7	0.04584	5.3	0.26	5.6	-11	128	247	7	263	5
10.1	582	594	21	1.02	0.0419	1.8	0.0127	3.1	0.05054	4.8	0.29	5.1	220	111	254	8	265	5
11.1	787	1079	29	1.37	0.0419	1.8	0.0127	2.2	0.04846	3.0	0.28	3.5	122	71	254	6	265	5
12.1	698	894	26	1.28	0.0425	1.8	0.0129	2.3	0.05121	2.7	0.30	3.2	250	62	260	6	268	5
13.1	511	489	18	0.96	0.0414	1.8	0.0127	2.7	0.04998	3.5	0.29	3.9	194	80	254	7	261	5
14.1	664	799	23	1.20	0.0407	1.8	0.0126	2.4	0.04926	3.4	0.28	3.9	160	80	253	6	257	5
15.1	638	702	23	1.10	0.0417	1.8	0.0128	2.3	0.05194	2.7	0.30	3.2	283	62	257	6	263	5
16.1	468	479	17	1.02	0.0406	1.9	0.0123	3.2	0.04983	6.6	0.28	6.9	187	155	247	8	257	5

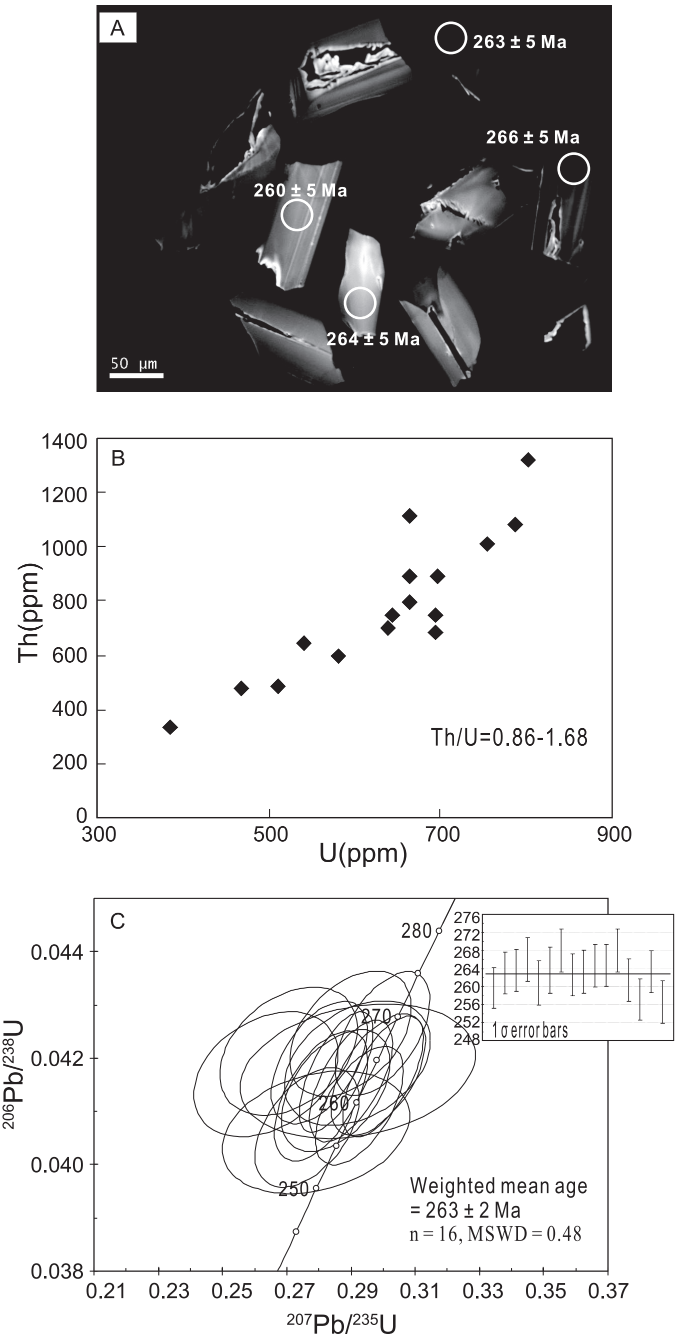

Fig. 3. (A) Cathodoluminescence (CL) image of representative zircons. Circle shows location of SHRIMP analyses with recorded ages. (B) Correlation of Th and U concentrations for the dated zircons. (C) SHRIMP zircon U-Pb concordia plot for Dashibao Formation basalt sample from the Baoxing area, Songpan-Ganzi Terrane. Inset shows 1 σ errors on the data.

Table 2

Major (%) and trace element ppm abundances of the Dashibao basalts from the Songpan-Ganzi Terrane, SW China

	Group1 (Alkaline basalts)						
	BX-1	BX-2	BX-3	BX-4	BX-4b	BX-8	BX-9
SiO_2	50.67	52.19	42.60	48.45	48.46	50.28	47.61
TiO_2	3.62	3.84	4.65	3.06	2.93	4.02	4.01
Al_2O_3	13.48	13.97	14.74	14.00	14.80	13.51	14.01
Fe_2O_3	13.15	11.69	13.89	12.21	13.05	12.82	13.34
MgO	4.47	5.15	5.40	5.66	4.35	4.96	4.65
CaO	7.48	3.19	9.10	7.85	10.02	6.94	8.23
Na_2O	2.27	0.03	0.49	2.54	1.97	2.86	2.03
K_2O	1.47	5.55	3.24	2.45	1.30	2.33	2.22
MnO	0.14	0.17	0.15	0.16	0.14	0.15	0.16
P_2O_5	0.37	0.17	0.31	0.32	0.31	0.42	0.43
LOI	3.40	3.19	4.80	2.85	2.41	2.18	3.47
Total	100.51	99.14	99.37	99.54	99.74	100.48	100.15
mg#	0.43	0.49	0.46	0.51	0.43	0.46	0.44
Sc	24.6	24.1	30.7	26.9	26.4	23.9	23.1
V	364	224	459	394	371	390	380
Cr	87.3	74.6	97.1	69.0	57.5	65.4	61.9
Co	41.8	37.1	39.5	45.8	40.1	40.7	45.2
Ni	79.4	83.2	65.0	49.6	44.6	83.0	89.9
Ga	23.5	21.5	33.6	23.2	22.3	24.3	27.8
Ge	2.09	2.64	2.81	2.28	1.73	1.74	2.08
Rb	29.90	111.6	67.28	41.94	18.34	57.12	50.48
Sr	802	50	1740	239	862	516	454
Y	32.93	27.85	43.42	30.17	27.25	35.97	36.98
Zr	326	375	436	279	265	359	383
Nb	35.30	37.93	44.06	27.66	26.49	39.12	39.15
Ba	216	421	321	430	300	615	453
La	42.19	50.80	43.34	34.61	34.12	49.82	51.93
Ce	94.07	104.20	115.60	78.64	77.67	108.90	111.60
Pr	12.94	12.39	15.84	11.12	10.31	15.05	15.50
Nd	53.46	49.12	65.35	45.76	41.17	60.50	62.86
Sm	10.38	9.64	13.67	9.19	8.57	11.68	12.23
Eu	3.10	2.67	5.63	2.64	2.71	3.27	3.84
Gd	9.23	8.72	12.48	8.33	7.89	10.11	10.64
Tb	1.40	1.34	1.89	1.23	1.14	1.53	1.57
Dy	7.24	7.17	9.83	6.47	5.95	7.95	8.25
Ho	1.28	1.30	1.71	1.18	1.11	1.41	1.46
Er	3.25	3.37	4.32	3.01	2.77	3.60	3.59
Tm	0.44	0.48	0.60	0.42	0.37	0.49	0.51
Yb	2.68	3.07	3.73	2.57	2.21	3.03	3.09
Lu	0.40	0.44	0.55	0.38	0.32	0.45	0.45
Hf	8.11	9.20	10.83	7.17	7.24	8.90	9.44
Ta	2.48	2.70	3.16	1.97	1.92	2.77	2.77
Pb	7.85	4.52	12.25	4.69	4.73	2.87	5.15
Th	6.94	7.54	8.63	5.21	5.12	7.50	7.75
U	1.15	0.83	1.29	1.11	1.11	1.55	1.70
La/Nb	1.20	1.34	0.98	1.25	1.29	1.27	1.33
Ti/Y	680	863	679	630	664	683	673

Table 2
(continued)

	Group1 (Alkaline basalts)						
	BX-9b	BX-10	BX-11	BX-12	BX-20	BX-22	BX-24
SiO_2	48.23	48.47	49.81	49.52	46.81	48.01	49.10
TiO_2	3.13	3.92	3.74	3.66	3.26	2.98	3.10
Al_2O_3	14.39	13.67	13.58	13.94	14.00	13.99	13.95
Fe_2O_3	13.39	13.35	12.56	13.82	15.20	12.50	12.73
MgO	4.61	5.06	4.87	4.49	7.50	5.57	4.75
CaO	9.21	7.90	7.67	5.22	3.19	8.29	7.50
Na_2O	2.12	2.38	2.38	2.75	0.20	3.37	2.97
K_2O	1.44	2.25	2.01	2.81	5.58	1.41	2.78
MnO	0.16	0.15	0.14	0.12	0.14	0.17	0.16
P_2O_5	0.33	0.43	0.41	0.40	0.31	0.33	0.35
LOI	2.85	3.10	2.88	3.02	4.06	2.49	2.18
Total	99.86	100.68	100.05	99.75	100.27	99.11	99.55
mg#	0.43	0.46	0.46	0.42	0.52	0.50	0.45
Sc	22.8	22.8	22.2	24.8	27.0	28.9	25.7
V	339	375	365	391	363	385	321
Cr	63.4	63.8	60.6	94.6	4.00	30.8	56.3
Co	40.5	43.8	40.4	42.2	37.2	42.4	42.9
Ni	79.0	85.9	78.3	78.3	20.7	60.2	55.1
Ga	23.1	25.8	23.6	25.5	22.1	20.8	20.0
Ge	1.74	1.88	1.78	1.66	1.58	2.33	2.02
Rb	48.39	41.66	34.01	49.29	46.91	33.24	24.66
Sr	621	397	276	159	76	467	404
Y	34.54	36.04	35.17	35.06	30.75	29.75	27.42
Zr	378	376	363	337	320	179	280
Nb	39.62	37.85	36.13	34.60	26.10	15.88	24.22
Ba	577	378	736	460	996	411	311
La	51.17	44.93	47.46	43.90	31.42	22.23	29.06
Ce	112.20	104.10	104.30	94.55	71.06	48.30	66.54
Pr	14.63	14.41	14.13	13.01	10.23	6.62	9.50
Nd	57.45	58.51	58.61	53.17	43.16	27.46	40.66
Sm	11.20	11.50	11.25	10.55	9.30	5.94	8.52
Eu	3.23	3.16	2.89	3.03	2.94	1.81	2.59
Gd	9.75	9.80	9.76	9.32	8.60	6.26	7.63
Tb	1.37	1.48	1.45	1.41	1.27	1.01	1.11
Dy	7.25	7.86	7.70	7.51	6.76	5.83	5.92
Ho	1.32	1.42	1.39	1.37	1.21	1.14	1.08
Er	3.41	3.61	3.52	3.52	3.11	3.13	2.75
Tm	0.44	0.50	0.49	0.49	0.43	0.46	0.37
Yb	2.72	3.13	3.04	2.99	2.68	2.96	2.31
Lu	0.39	0.46	0.45	0.45	0.40	0.46	0.35
Hf	10.32	9.54	9.15	8.65	7.62	4.64	7.03
Ta	2.80	2.72	2.62	2.50	1.87	1.12	1.73
Pb	4.30	5.93	5.54	5.43	4.54	5.68	4.80
Th	8.01	7.50	7.38	6.84	4.58	3.56	3.96
U	1.78	1.68	1.63	1.49	0.30	0.85	0.92
La/Nb	1.29	1.19	1.31	1.27	1.20	1.40	1.20
Ti/Y	561	669	657	648	661	621	696

Table 2

(continued)

	Group2 (Tholeiitic basalts)						
	BX-5	BX-6	BX-7	BX-13	BX-13b	BX-14	BX-15
SiO_2	51.65	48.29	49.89	50.64	47.26	50.27	49.30
TiO_2	2.19	2.44	2.41	2.26	1.99	2.42	2.05
Al_2O_3	13.91	14.06	13.67	13.93	15.15	13.95	13.96
Fe_2O_3	11.64	14.05	13.47	13.73	13.04	12.84	14.28
MgO	6.33	5.21	5.19	4.95	5.50	5.51	6.18
CaO	5.72	7.97	7.51	7.99	10.13	6.49	4.98
Na_2O	3.65	2.66	3.72	3.14	2.65	4.06	1.97
K_2O	0.04	1.03	0.92	1.51	0.76	1.09	0.49
MnO	0.15	0.19	0.18	0.16	0.17	0.16	0.15
P_2O_5	0.25	0.32	0.32	0.27	0.19	0.33	0.27
LOI	4.32	2.78	2.49	2.12	3.47	2.87	6.47
Total	99.85	99.00	99.75	100.68	100.29	99.99	100.09
mg#	0.44	0.48	0.49	0.49	0.52	0.57	0.42
Sc	26.3	34.8	35.3	34.8	27.7	33.4	30.0
V	309	458	438	458	298	444	416
Cr	46.8	92.6	81.4	92.6	52.3	89.3	34.3
Co	48.7	43.2	39.2	43.2	47.1	48.2	35.2
Ni	78.9	60.2	54.0	60.2	86.3	57.4	60.1
Ga	19.4	21.2	18.9	21.2	19.4	19.6	20.5
Ge	2.17	1.68	1.45	1.68	1.53	1.69	2.75
Rb	0.80	19.36	26.11	19.36	12.19	17.36	21.34
Sr	521	941	442	941	262	171	136
Y	25.32	34.79	33.51	34.79	22.69	36.69	29.41
Zr	197	242	226	242	196	225	175
Nb	12.00	18.58	18.07	18.58	12.01	18.37	20.16
Ba	85.3	464	382	464	223	251	160
La	22.62	26.58	23.98	26.58	20.77	24.77	27.53
Ce	51.68	57.19	54.68	57.19	48.03	56.15	56.74
Pr	7.31	8.06	7.78	8.06	6.76	7.96	7.56
Nd	31.19	33.81	33.33	33.81	28.09	35.50	30.24
Sm	6.78	7.34	7.12	7.34	6.27	7.43	6.13
Eu	2.05	2.23	2.10	2.23	2.04	2.31	1.82
Gd	6.27	7.33	7.26	7.33	5.79	7.72	6.22
Tb	0.97	1.18	1.15	1.18	0.89	1.23	1.03
Dy	5.37	6.78	6.66	6.78	4.66	7.03	5.83
Ho	0.98	1.33	1.28	1.33	0.90	1.35	1.14
Er	2.59	3.56	3.46	3.56	2.30	3.62	3.03
Tm	0.36	0.52	0.50	0.52	0.31	0.52	0.46
Yb	2.24	3.33	3.20	3.33	1.90	3.35	2.96
Lu	0.34	0.52	0.51	0.52	0.28	0.53	0.46
Hf	4.90	5.80	5.74	5.80	5.06	5.74	4.33
Ta	0.85	1.24	1.23	1.24	0.81	1.23	1.36
Pb	2.13	3.31	2.20	3.31	4.49	4.36	2.30
Th	2.41	3.42	3.42	3.42	2.16	3.48	5.01
U	0.50	0.70	0.73	0.70	0.47	0.71	1.56
La/Nb	1.89	1.43	1.33	1.34	1.73	1.35	1.37
Ti/Y	542	438	443	516	543	408	447

TABLE 2

(continued)

	Group2 (Tholeiitic basalts)							
	BX-16	BX-17	BX-18	BX-18b	BX-19	BX-21	BX-23	BX-25
SiO_2	49.61	50.17	44.51	47.22	45.69	49.06	47.36	47.74
TiO_2	2.09	1.73	2.28	2.21	2.18	1.99	1.87	1.87
Al_2O_3	13.94	13.95	14.62	15.73	14.40	13.96	13.98	13.97
Fe_2O_3	12.97	11.25	15.80	13.18	14.70	12.91	13.84	12.72
MgO	6.29	6.63	5.23	6.59	5.50	5.41	6.12	6.71
CaO	9.71	8.06	6.71	8.39	7.57	8.62	9.73	9.15
Na_2O	2.29	3.52	2.91	2.87	3.16	2.85	3.27	2.91
K_2O	0.65	0.76	0.03	0.69	0.10	1.81	0.53	0.80
MnO	0.18	0.16	0.20	0.16	0.19	0.17	0.21	0.18
P_2O_5	0.20	0.17	0.28	0.26	0.25	0.24	0.17	0.20
LOI	2.81	2.83	7.86	2.48	7.18	2.77	2.61	2.77
Total	100.75	99.22	100.44	99.76	100.91	99.79	99.70	99.01
mg#	0.53	0.45	0.55	0.45	0.46	0.48	0.50	0.54
Sc	29.5	29.8	28.4	30.4	26.1	38.2	26.0	26.3
V	372	328	520	225	473	394	328	309
Cr	112	172	30.5	5.48	41.0	47.4	38.6	46.8
Co	52.6	52.0	56.1	39.5	53.5	54.8	43.5	48.7
Ni	92.6	106	64.7	4.07	62.8	62.4	51.0	78.9
Ga	20.3	18.6	22.3	22.4	19.5	18.5	20.4	19.4
Ge	2.05	1.76	2.64	2.31	1.83	1.97	1.74	2.17
Rb	20.68	24.47	3.26	12.74	7.20	13.3	52.3	0.80
Sr	640	427	3206	239	993	273	401	521
Y	24.44	20.10	24.54	37.56	22.91	26.0	28.4	25.32
Zr	164	115	148	287	141	129	304	197
Nb	13.37	10.69	16.91	28.00	17.29	13.79	25.50	12.00
Ba	247	283	1769	299	166	301	384	85.3
La	19.48	15.94	23.90	34.59	21.99	14.00	31.71	22.62
Ce	43.95	35.64	50.17	78.87	47.30	32.22	71.84	51.68
Pr	6.23	5.09	6.92	10.65	6.52	4.67	10.12	7.31
Nd	26.83	22.63	29.05	44.55	27.13	20.31	42.65	31.19
Sm	5.78	4.83	6.03	9.68	5.73	4.76	8.87	6.78
Eu	1.82	1.63	1.97	3.16	1.81	1.68	2.72	2.05
Gd	5.90	4.83	6.32	9.49	5.64	5.35	8.14	6.27
Tb	0.89	0.75	0.95	1.38	0.86	0.89	1.17	0.97
Dy	4.96	4.25	5.11	7.57	4.74	5.20	6.02	5.37
Ho	0.93	0.77	0.96	1.47	0.89	0.99	1.09	0.98
Er	2.42	1.97	2.40	3.75	2.26	2.64	2.77	2.59
Tm	0.34	0.28	0.33	0.51	0.32	0.39	0.38	0.36
Yb	2.10	1.74	2.13	3.14	1.98	2.45	2.43	2.24
Lu	0.32	0.26	0.32	0.48	0.30	0.38	0.37	0.34
Hf	4.01	2.92	3.67	7.64	3.46	3.21	7.23	4.90
Ta	0.94	0.75	1.15	1.94	1.14	0.95	1.82	0.85
Pb	2.93	2.76	3.19	2.85	2.90	2.53	4.84	2.13
Th	2.45	1.97	2.74	4.66	2.70	1.79	4.09	2.41
U	0.52	0.40	0.62	1.07	0.60	0.41	0.90	0.50
La/Nb	1.46	1.49	1.41	1.24	1.27	1.02	1.24	1.31
Ti/Y	525	535	603	363	609	474	407	492

LOI: Loss on ignition, *mg#* = $Mg^{2+}/(Mg^{2+}+Fe^{2+})$ in atomic ratio; the data of Group 1 samples are from Zi and others (2008a). Note that relative position in the stratigraphy is given in Fig. 11.

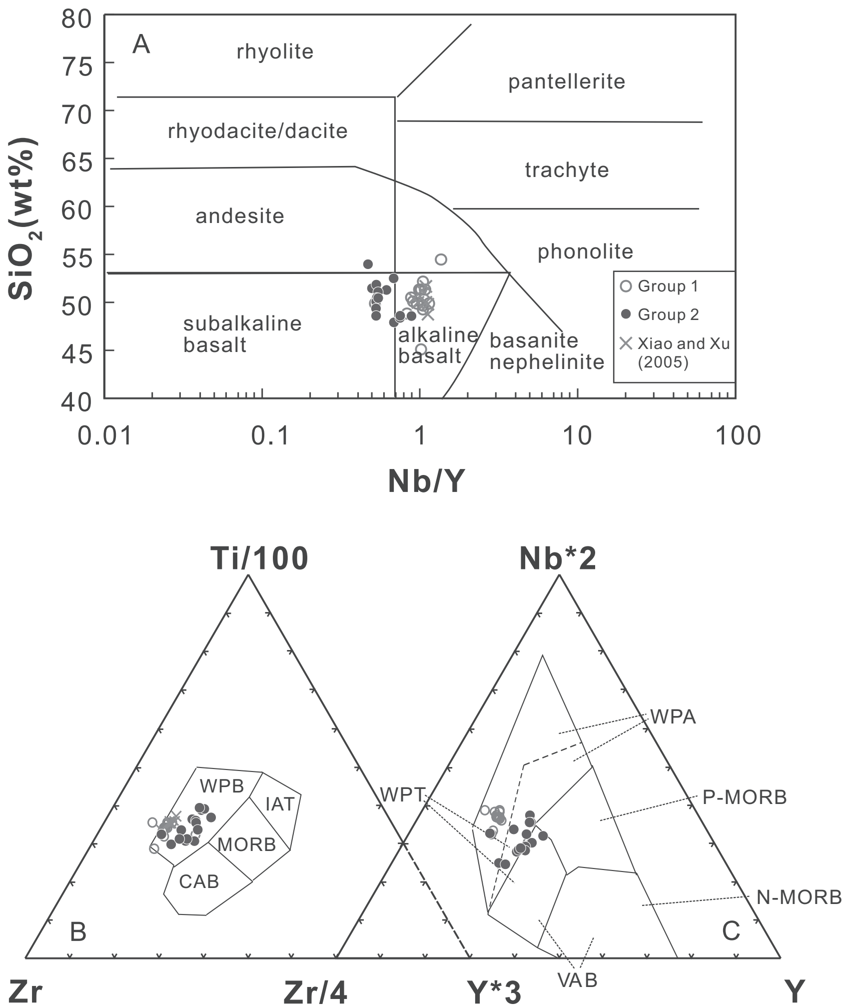

Fig. 4. Discrimination diagrams for the Dashibao Formation basalts. (A) SiO_2 vs. Nb/Y (after Winchester and Floyd, 1977). (B) Ti-Zr-Y (after Pearce and Cann, 1973), WPB: within-plate basalts, IAT: island-arc tholeiites, CAB: calc-alkaline basalts, MORB: mid-ocean ridge basalts. (C) Nb-Zr-Y (after Meschede, 1986), WPA: within-plate alkali basalts, WPT: within-plate tholeiites, P-MORB: P-type mid-ocean ridge basalts, N-MORB: N-type mid-ocean ridge basalts, VAB: volcanic arc basalts. Data of Xiao and Xu (2005) are also plotted. Symbols in (B) and (C) are the same as in figure 4A.

the Emeishan high-Ti lavas (Xu and others, 2001; Zhang and Wang, 2002; Xiao and others, 2004; Zhang and others, 2006). Group 2 tholeiitic basalts display a flatter pattern and lower light REE contents, and have lower Sm/Yb ratios than Group 1 alkaline basalts. None of the analyzed samples show significant europium anomalies, with Eu* values ranging from 0.82 to 1.29 and from 0.88 to 1.02 for groups 1 and 2, respectively (figs. 7A and 7B). On primitive-mantle normalized spider diagrams (figs. 7C and 7D), the two groups exhibit enrichment in LILE, and again have patterns analogous to those of OIB and the Emeishan high-Ti basalts (Xu and others, 2001; Zhang and Wang, 2002; Xiao and others, 2004; Zhang and others, 2006). Group 1 basalts are strongly enriched in incompatible trace elements, comparable with OIB, but both groups are lower in Nb and Ta than ocean island basalts (Sun and

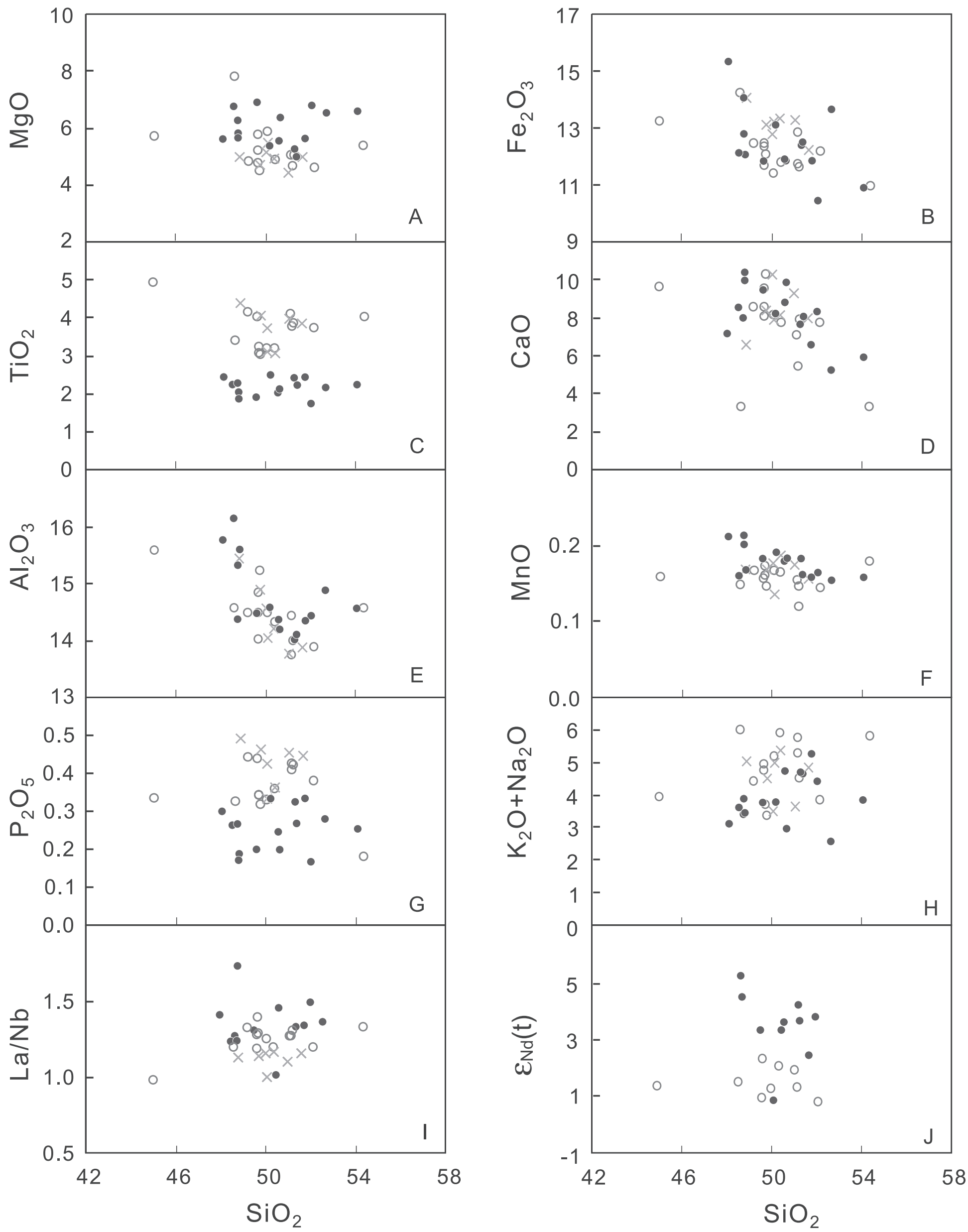

Fig. 5. Selected Harker variation diagrams for the Dashibao Formation basalts. Symbols are the same as in figure 4A.

McDonough, 1989) and display negative Sr anomalies and $(Nb/La)_n$ ratios ranging from 0.51 to 0.98.

Sr and Nd isotopic ratios and abundances of the Dashibao basalts are listed in table 3. The initial isotopic ratios were corrected to 263 Ma. The basalts possess weakly to moderately positive $\varepsilon_{Nd}(t)$ values varying from +0.82 to +5.28, similar to those of the Emeishan high-Ti series (table 3 and fig. 8; Song and others, 2001; Xu and others,

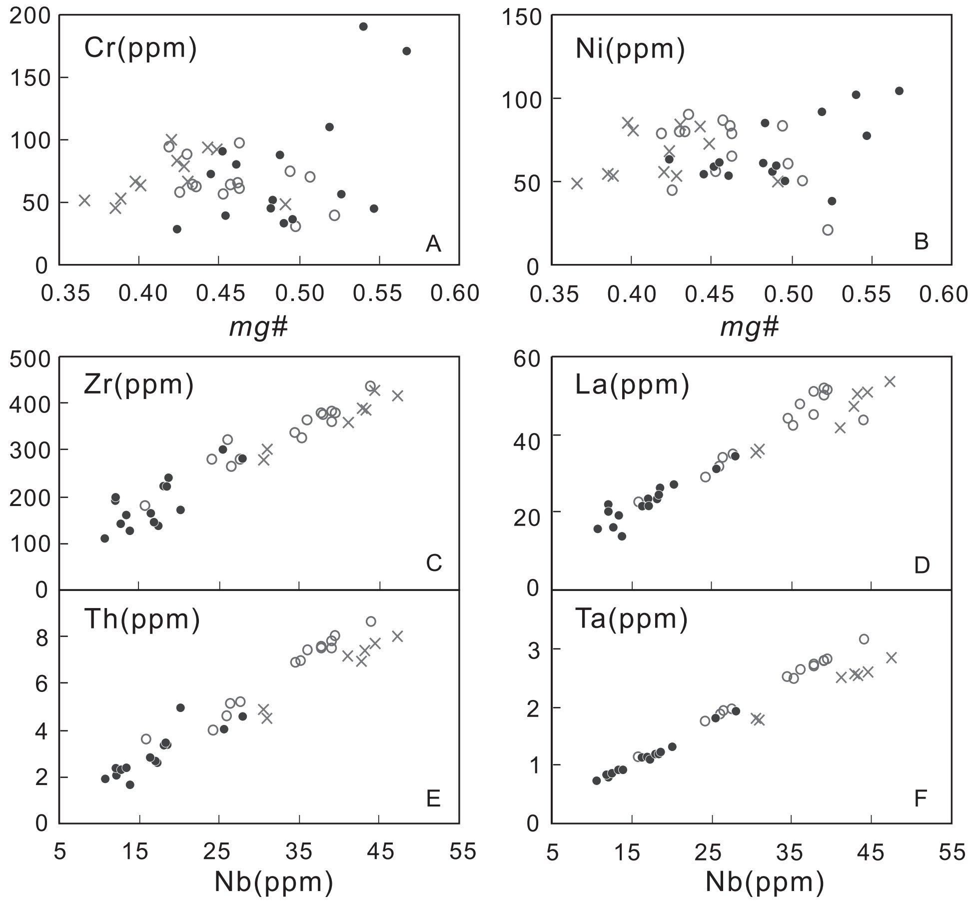

Fig. 6. Plots of Cr and Ni vs. *mg#* (A and B) and Zr, La, Th and Ta vs. Nb (C-F) for the Dashibao Formation basalts. Symbols are the same as in figure 4A.

2001; Xiao and others, 2004; Zhang and others, 2006). Generally, Group 1 alkaline basalts have less positive $\varepsilon_{Nd}(t)$ values than their tholeiitic counterparts in Group 2. The initial Sr isotopic ratios $((^{87}Sr/^{86}Sr)_i)$ range from 0.704852 to 0.707779 and display a considerable scatter, possibly due to mobility of Rb during surface processes.

DISCUSSION AND CONCLUSIONS

Post-magmatism Alteration and Crystal Fractionation

The Dashibao Formation basalts were extruded in a submarine environment and were subsequently metamorphosed to lower greenschist facies during post-eruption tectonothermal events (Huang and others, 2003), and hence could have been subjected to mobilization of primary elemental concentrations. Some variations in highly incompatible elements (for example, Rb, Sr, Ba and K) and high LOI values (2.12-7.86 wt. %, table 2) suggest alteration and some degree of mobility. However, the samples show no significant correlations between Rb and Nb concentrations, which together with positive correlations between moderately incompatible elements (Zr, La, Th, Ta, figs. 6C-F), imply that the highly incompatible elements (for example, Rb, Ba and K) might have been mobile whereas the moderately incompatible elements have been

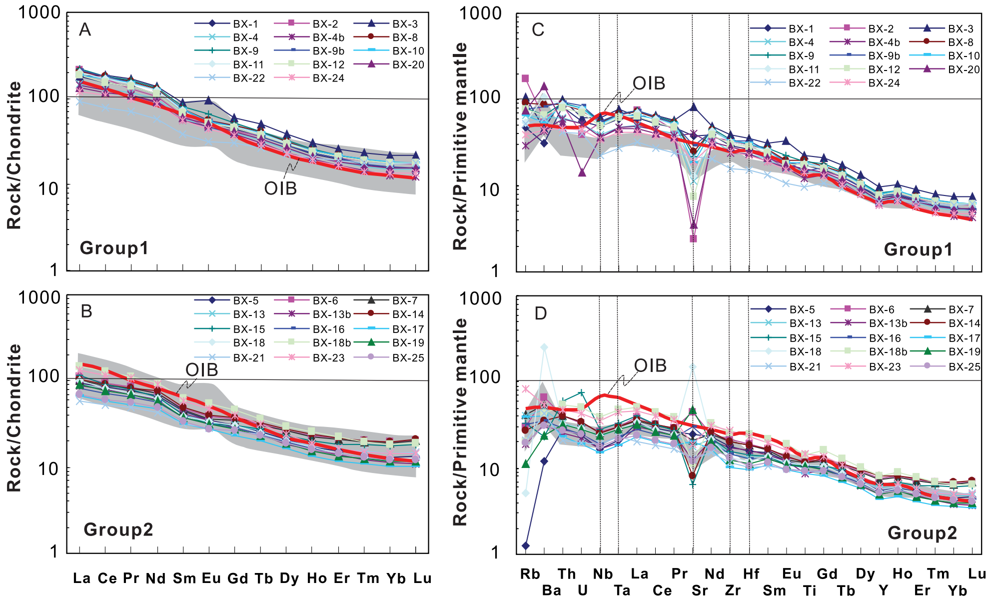

Fig. 7. Chondrite-normalized REE patterns of (A) Group 1 and (B) Group 2 and primitive mantle-normalized spidergrams of (C) Group 1 and (D) Group 2 for the Dashibao Formation basalts. Normalized values for chondrite and primitive mantle are from Taylor and McLennan (1985) and Sun and McDonough (1989), respectively. The shaded areas show ranges of the typical Emeishan high-Ti basalts, data from Xu and others (2001) and Xiao and others (2004).

immobile during low-temperature alteration (Frey and others, 1994; Hollanda and others, 2006). In addition, as shown in the $\varepsilon_{Nd}(t)$ vs. $(^{87}Sr/^{86}Sr)_i$ plot (fig. 8), the high $(^{87}Sr/^{86}Sr)_i$ variation with relatively high LOI (for example, BX-19) indicates that the Rb-Sr isotope system has been affected by alteration. Therefore, we mainly consider Nd isotopic ratios when discussing the petrogenesis of the samples.

The low Ni and Cr contents and *mg*# of the samples suggest that they have undergone considerable crystal fractionation. The generally negative correlations between major oxides and SiO_2 and the overall positive correlations between Ni and Cr with *mg*# for Group 2 (see figs. 5, 6A and 6B) indicate fractionation of olivine and clinopyroxene. The absence of a strong negative correlation between TiO_2 and SiO_2 (fig. 5C) and the small depletions of Ti (figs. 7C and 7D) argue against significant fractionation of Ti-Fe oxides in the early evolution of the magmas. Although a number of the samples display a negative Sr anomaly (fig. 7), the lack of negative Eu anomalies (figs. 7A and 7B) and positive correlation between *mg*# and Sr precludes significant fractionation of plagioclase. The variable Sr anomalies of these rocks (figs. 7C and 7D) might be attributed to the post-magmatic alteration.

Lithosphere Signature and Crustal Contamination

Low-Ti basalts, including those associated with many continental flood basalts and volcanic arc basalts generally exhibit trace element ratios that strongly differ from those of oceanic basalts (OIB and MORB), and their signatures have been interpreted as the imprint of subcontinental lithospheric mantle (SCLM) derived melts (Lightfoot and others, 1993; Garland and others, 1996). The SCLM is often modified by fluids related to dehydration in subduction zones (Noll and others, 1996) and may have incorporated subducted sediments (Sun and McDonough, 1989). These processes induce relative depletions in Ti, P, Nb and Ta and relative enrichments in Pb and Ba.

Table 3

Sr and Nd isotopic compositions of the Dashibao basalts from the Songpan-Ganzi Terrane, SW China

Sample	Sm	Nd	Rb	Sr	$^{147}Sm/^{144}Nd$	$^{143}Nd/^{144}Nd\pm2\sigma$	$^{87}Rb/^{86}Sr$	$^{87}Sr/^{86}Sr\pm2\sigma$	$(^{87}Sr/^{86}Sr)_i$	$\varepsilon_{Nd}(t)$
Group1										
BX-1	10.38	53.46	29.9	801.7	0.117	0.512545 ±8	0.108	0.706557±18	0.706157	0.82
BX-3	13.67	65.35	67.28	1740.4	0.127	0.512590±10	0.112	0.706194±20	0.705779	1.39
BX-4	9.19	45.76	41.94	239.4	0.121	0.512577±12	0.508	0.707045±19	0.705166	1.31
BX-8	11.68	60.50	57.12	515.8	0.117	0.512602±16	0.321	0.707040±18	0.705852	1.95
BX-10	11.50	58.51	41.66	396.7	0.119	0.512556±12	0.304	0.706924±18	0.705798	0.98
BX-11	11.25	58.61	34.01	276.3	0.120	0.512570 ±8	0.357	0.707345±20	0.706025	1.35
BX-20	9.30	43.16	46.91	76.0	0.130	0.512603±12	1.790	0.711460±20	0.704837	1.52
BX-22	8.52	40.66	24.66	404.4	0.127	0.512639±16	0.177	0.706729±19	0.706075	2.35
BX-24	8.87	42.65	52.27	401.1	0.126	0.512624±10	0.378	0.706884±16	0.705487	2.08
Group2										
BX-6	7.34	33.81	19.36	940.9	0.131	0.512571 ±9	0.060	0.707257±25	0.707036	0.87
BX-7	7.12	33.33	26.11	442.4	0.129	0.512741±13	0.171	0.706190±19	0.705557	4.25
BX-13	6.30	29.08	25.35	373.3	0.127	0.512715±11	0.197	0.705580±18	0.704852	3.69
BX-14	7.43	35.50	17.36	170.7	0.123	0.512645 ±9	0.295	0.705988±17	0.704897	2.46
BX-16	5.78	26.83	20.68	640.0	0.130	0.512710±30	0.094	0.707136±20	0.706789	3.61
BX-17	4.83	22.63	24.47	427.2	0.129	0.512718±10	0.166	0.707225±17	0.706611	3.81
BX-19	5.73	27.13	7.196	992.8	0.128	0.512791±15	0.021	0.707857±17	0.707779	5.28
BX-21	5.94	27.46	33.24	466.9	0.131	0.512698±10	0.206	0.706609±17	0.705846	3.36
BX-23	4.76	20.31	13.25	272.9	0.142	0.512777±12	0.141	0.705778±19	0.705257	4.54
BX-25	5.14	23.03	12.32	255.2	0.135	0.512704 ±8	0.140	0.705441±17	0.704923	3.33

Chondrite uniform reservoir values, $^{147}Sm/^{144}Nd = 0.1967$, $^{143}Nd/^{144}Nd = 0.512638$, are used for the calculation. $\varepsilon_{Nd}(t)$ is calculated by assuming 263 Ma.

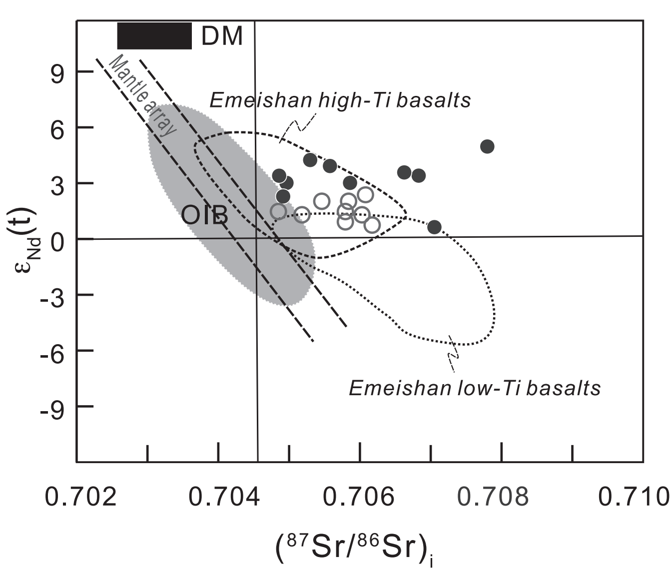

Fig. 8. $\varepsilon_{Nd}(t)$ vs. $(^{87}Sr/^{86}Sr)_i$ diagram for the Dashibao Formation basalts. Data source: DM (depleted mantle) and OIB (oceanic island basalt), Sun and McDonough (1989); Emeishan high- and low-Ti basalts, Xu and others (2001), Xiao and others (2004) and Zhang and others (2006). Symbols are the same as in figure 4A.

Moreover, hydration of the SCLM lowers its solidus, permitting higher degrees of melting (Gallagher and Hawkesworth, 1992). Some authors have proposed that the lithospheric signature of many continental flood basalts may simply be produced by crustal contamination of asthenospheric magmas en route to the surface (Arndt and others, 1993; Wooden and others, 1993). Indeed, the strong enrichment in continental crust in Pb and Ba and its depletion in Nb, Ta, and Ti and the relative depletion of high field strength elements (HFSE), especially Nb and Ta, in continental lavas, could result from interactions between the SCLM and asthenospheric melts (for example, Bodinier and others, 1996). The crystallization of HFSE-bearing oxides, during the percolation of melts through the lithospheric mantle would decrease the budget of these melts relative to other elements.

Xiao and others (2004) argued that the Emeishan Low-Ti series lavas with relatively high La/Nb ratios contain a significant contribution from the SCLM. In the case of the Dashibao Formation, the basalts have variable La/Nb ratios that are generally greater than 1 (table 2). Group 2 basalts as a whole have higher La/Nb ratios than those in Group 1 and all of them exhibit a notable Nb trough on the spidergram (fig. 7D), so it seems that lithospheric mantle components were involved in generation of the Group 2 magmas. However, the influence of the lithosphere component gradually lessened with time, and the late stage Group 1 alkaline magmas have probably experienced the least lithospheric contamination, consistent with their lower La/Nb ratios (table 2) and more typical OIB geochemical features than Group 2 basalts (fig. 7).

Elevated SiO_2 contents, high initial $^{87}Sr/^{86}Sr$ ratios, low $\varepsilon_{Nd}(t)$ values and negative Nb and Ta anomalies are commonly used as indicators of crustal contamination of mafic melts (DePaolo, 1981). The Dashibao Formation basalts exhibit weak correlations between SiO_2 (and TiO_2) and Nd isotopic compositions (fig. 5J), and no prominent linear correlation between La/Nb ratios and SiO_2 contents (fig. 5I). Consequently, assimilation and fractional crystallization (AFC) processes are not considered to have been significant in generation of the basalts.

Mantle Source and Partial Melting

Thick low-Ti lavas occupy stratigraphically lower levels mainly along the western part of the Emeishan LIP, and the overlying high-Ti basalts are the dominant rock type in the outer zone of the province (Xu and others, 2001). Such a spatial distribution of magma types could originate from a composite plume-lithosphere interaction (Chung and Jahn, 1995; Zhang and Wang, 2002; Xiao and others, 2004; Fan and others, 2008; Song and others, 2008). The Dashibao basalts predominantly plot in the within-plate field with Group 1 corresponding to the within-plate alkaline basalt whereas the majority of Group 2 fall in the superimposed area of within-plate alkaline and tholeiitic basalts (figs. 4B and 4C). The basalts, especially the alkaline group (Group 1), display strong enrichment in LILE and HFSE, and show OIB-type REE and trace element patterns, similar to the plume-derived high-Ti basalt of the Emeishan LIP (figs. 7A-D).

Dashibao Formation tholeiitic basalts (Group 2) display trace element compositions intermediate between those of Group 1 alkaline and Emeishan low-Ti basalts. In the Th/Yb vs. Ta/Yb plot (fig. 9), some exhibit Th/Yb and Ta/Yb ratios similar to those of the Group 1 and/or Emeishan high-Ti magmas, whereas others exhibit a shift towards the Emeishan low-Ti and depleted mantle source. The Dashibao basalt samples possess OIB-like Nd isotopic compositions similar to the Emeishan basalts, but record a narrow $\varepsilon_{Nd}(t)$ range relative to the latter (fig. 8), suggesting that mantle plume material likely made a dominant contribution to the generation of the parental magmas. The $\varepsilon_{Nd}(t)$-$(^{87}Sr/^{86}Sr)_i$ diagram (fig. 8) also shows Group 1 alkaline basalts from the Dashibao Formation plot within the field of the Emeishan high-Ti series. However, the isotopic compositions of Group 2 tholeiitic basalts are not as enriched as

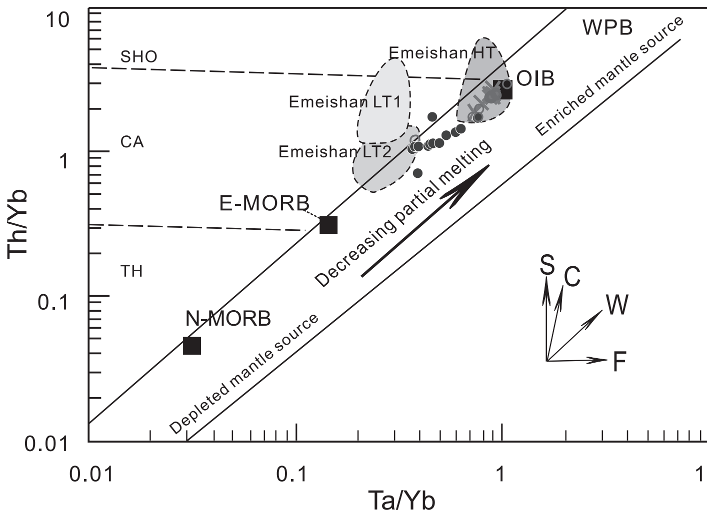

Fig. 9. Th/Yb vs. Ta/Yb plot (after Pearce, 1983) for the Dashibao Formation basalts. Vectors indicate the influence of subduction components (S), within-plate enrichment (W), crustal contamination(C), and fractional crystallization (F). Dashed lines separate the boundaries of the tholeiitic (TH), calc-alkaline (CA), and shoshonitic (SHO) fields. Values of N-MORB, E-MORB, OIB and WPB are from Sun and McDonough (1989). Also plotted are Emeishan high-Ti (HT) and low-Ti (LT1 and LT2) basalts, data from Xu and others (2001), Xiao and others (2004) and Zhang and others (2006). Symbols are the same as in figure 4A.

the most primitive low-Ti series at Emeishan; by contrast, they possess relatively more depleted $\varepsilon_{Nd}(t)$ values when compared with Group 1 alkaline samples as well as most of the Emeishan flood lavas (table 3 and fig. 8), which cannot be explained by lithospheric contamination, but likely reflects plume source heterogeneity or additional involvement of a depleted mantle component in their genesis.

Input of variable proportions of MORB-like depleted component into an incipient OIB-type mantle source has been invoked to account for isotope differences between the Hawaiian tholeiites and alkalic basalts (Chen and Frey, 1983). Such interactions between depleted asthenosphere and mantle plumes have been postulated based on seismic investigations (for example, Gaherty, 2001; Montagner and Ritsema, 2001). The western margin (current coordinates) of the Yangtze Block was a passive continental shelf during the Permian and Middle Triassic times. Significant extension in the Late Permian affected the local lithosphere, resulting in the formation of a narrow basin floored by oceanic lithosphere and termed the Ganzi-Litang ocean (Chung and others, 1998 and references therein). Given such a regional tectonic setting creating the Dashibao marine basalts, along with the similarity of magma type distribution [that is, tholeiitic basalts overlain by late stage alkaline lavas (Macdonald and Katsura, 1964)], the Hawaiian model may also apply to the Dashibao basalts.

The Dashibao Formation basalts could correspond to partial melts of the Emeishan mantle plume. Group 1 alkaline basalts display high incompatible trace element contents that are characteristic of magmas formed by low degrees of partial melting. A plot of Sm/Yb vs. La/Yb (fig. 10A) enables differentiation between the melting of spinel and garnet peridotite because the heavy REE Yb is compatible in garnet, whereas La and Sm are incompatible, such that La/Yb and Sm/Yb will be strongly fractionated when the degree of melting is low. In contrast, La/Yb is only slightly fractionated and Sm/Yb is nearly unfractionated during melting in the spinel stability field. Figure 10A shows that variable degrees (5-19%) of batch melting of a hypotheti-

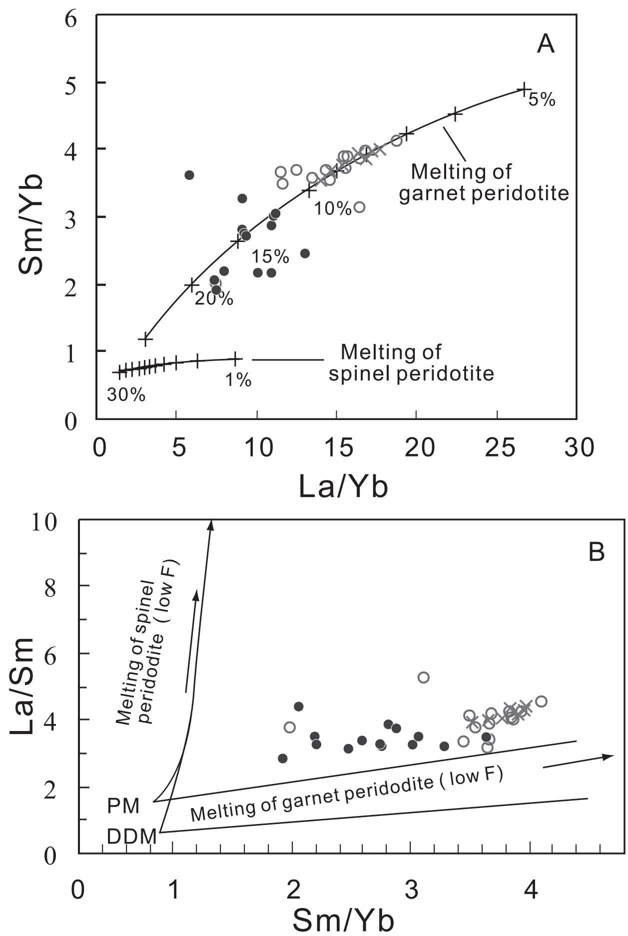

Fig. 10. (A) Sm/Yb vs. La/Yb plot for the Dashibao Formation basalts. Also shown are batch melting curves calculated for garnet peridotite and spinel peridotite. Partition coefficients are taken from Johnson and others (1990). The starting materials are ol, 55%; opx, 20%; cpx, 15%; gt, 10%; melting reaction in garnet field (Walter, 1998): ol, 3%; opx, 3%; cpx, 70%; gt, 24%; melting reaction in spinel field (Kinzler, 1997): ol, −6%; opx, 28%; cpx, 67%; sp, 11%. (B) La/Sm vs Sm/Yb plot (after Lassiter and DePaolo, 1997) for the Dashibao Formation basalts, PM—primary mantle (McKenzie and O'Nions, 1991); DMM—depleted mantle (McKenzie and O'Nions, 1991). Symbols are the same as in figure 4A.

cal light REE-enriched mantle source ((La/Yb)n >1) in the garnet stability field can generate the La/Yb-Sm/Yb systematics of Dashibao Formation basalts. Specifically, the Group 1 alkaline basalts could have been formed by 5 to 11 percent melting of garnet peridotite, whereas the Group 2 tholeiitic magmas correspond to higher degrees of melting of 13 to 19 percent. This is also in agreement with the trend shown by the La/Sm vs. Sm/Yb plot (fig. 10B).

Model Relating Dashibao Lavas to Emeishan LIP

The U-Pb age of 263 ± 2 Ma obtained from the Dashibao basalt in Baoxing county is identical within error to the Emeishan LIP age (~260 Ma), constrained largely by U-Pb dating of mafic and felsic intrusions (for example, Zhou and others, 2002; Guo and others, 2004; Xu and others, 2008), which, combined with geochemical data, suggests the Dashibao Formation lavas originated from Emeishan plume activity.

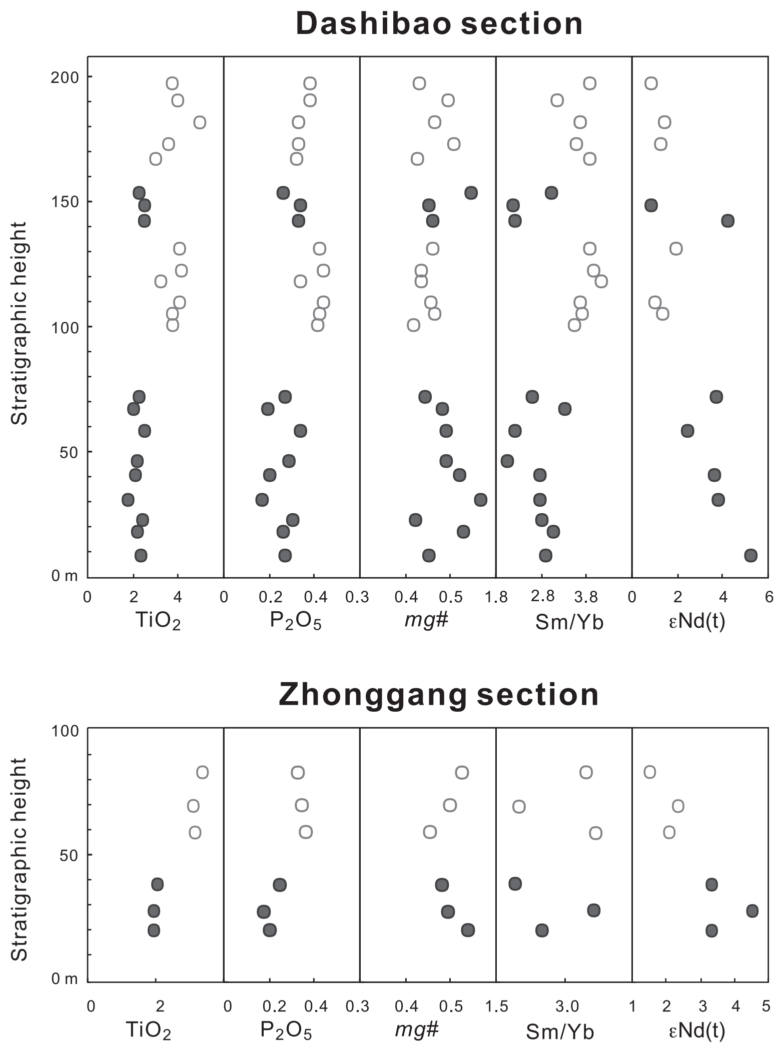

Fig. 11. Chemostratigraphic columns showing vertical variation of geochemical parameters for the Dashibao Formation basalts, which are divided into Group 1 and Group 2. Symbols are the same as in figure 4A. Location of sample sites given in figure 2.

The Dashibao basalts crop out within the Songpan-Ganzi Terrane, to the west of the Yangtze Block but are geochemically comparable with the Emeishan high-Ti basalts and the associated high-Ti intrusions that lie within the Yangtze Block (Xu and others, 2001; Xiao and others, 2004; Zhou and others, 2008; Zi and others, 2008b). As discussed above, the REE and incompatible elemental variation may reflect different degrees of melting of garnet-bearing mantle, with the Dashibao basalts likely generated at the periphery of the plume, which resulted in low-degree melting of plume materials, as has been recorded in laboratory experiments and by numerical modeling (Griffiths and Campbell, 1990).

Chemostratigraphic columns of the Dashibao lava sequence indicate that there was a temporal progression from Group 2 upwards to Group 1 magmas (fig. 11); similar variation has been observed in the adjacent Yangliuping basalts (Song and

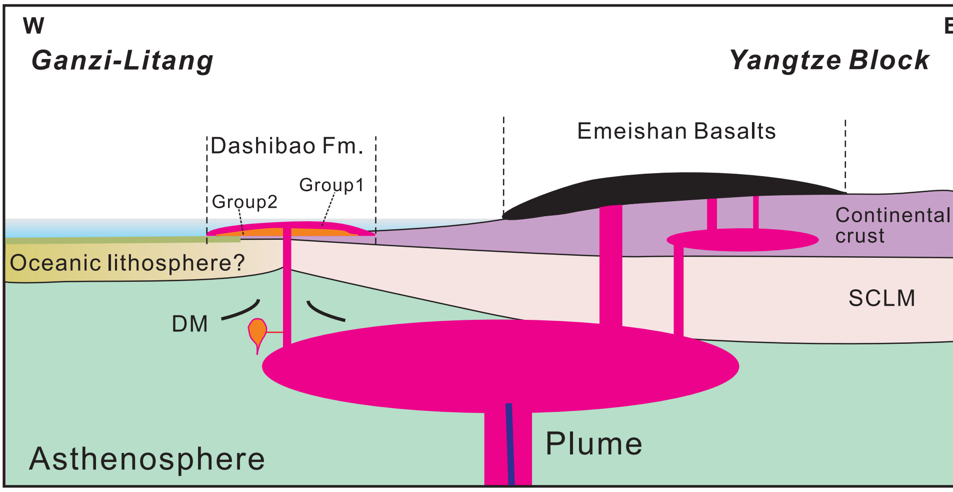

Fig. 12. Model for the origin of the Dashibao Formation Group 1 and Group 2 basalts, illustrating that they were derived from mantle sources related to the Emeishan plume.

others, 2006). This compositional shift cannot be explained simply in terms of partial melting or lithospheric contamination of a mantle derived melt. Instead, taking into account the tectonic context creating the Dashibao basalts, we favor a scenario where the petrogenesis of the early stage Group 2 tholeiitic lavas involved a depleted mantle source in addition to the input of plume-derived parental magmas, as has been documented in the Hawaiian hotspot basalts (Chen and Frey, 1983).

Based on our geochemical data, we propose a model to explain the origin and compositional variations of the Dashibao Formation basalts. The primitive magmas were generated by partial melting of the OIB-type Emeishan mantle plume, and then mixed with a proportion of depleted mantle material that may have originated from ambient depleted mantle entrained during the ascent of the plume (fig. 12). The strong REE fractionation is attributed to partial melting of a plume-derived basaltic source, leaving garnet as a residual phase. The addition of a depleted mantle component to the primitive plume melts would thus have produced basaltic magmas with an unradiogenic Nd composition, as revealed by the depleted Nd isotopic signature of the Group 2 basalts. The late stage alkaline magmas (Group 1) were derived from a deeper level of the mantle plume source through lower degrees of partial melting relative to the early stage tholeiitic basalts. The relatively high Sm/Yb ratio shown by these magmas, suggests higher pressure melting. It should be noted that the petrogenetic processes giving rise to the Dashibao Formation basalts are likely to be considerably more complex than the model outlined above, however the model adequately explains the systematic variations in incompatible element abundances and isotopic ratios.

Implications for the Age of the Emeishan Volcanism: A Boundary Event?

Previous direct U-Pb dating of the Emeishan basalts has been limited and has focused on the intrusive phases of the LIP. ^{40}Ar-^{39}Ar dating of extrusive phases has only had limited success due to tectonothermal overprinting and has yielded a variety of ages ranging from ~259 Ma to 41 Ma (Boven and others, 2002; Lo and others, 2002; Ali and others, 2004; Fan and others, 2004). U-Pb dating of zircons from mafic sills in the Inner Zone of the LIP, which were taken as part of the feeder system of the main mafic eruptive phase, yielded a $^{206}Pb/^{238}U$ age of 259 ± 3 Ma (Zhou and others, 2002). Guo and others (2004) recorded a U-Pb zircon age of 262 ± 3 Ma from dikes that intruded Devonian strata in western Sichuan, which they interpreted as marking the onset of the Emeishan mantle plume activity. More U-Pb dates from mafic and felsic intrusions associated with the Emeishan LIP have been published in recent years, and generally clustered at ~260 Ma (Zhou and others, 2006; Shellnutt and Zhou, 2007, 2008; Xu and others, 2008; Zhou and others, 2008). Also, some younger U-Pb ages of ~ 251 Ma from felsic plutons in the center of the LIP have been reported (Zhong and others, 2007; Shellnutt and Zhou, 2008). Nevertheless, the ages obtained from the intrusions may not represent that of the flood basalts formed by the Emeishan volcanic activity.

Since a genetic relation between the Dashibao and the Emeishan basalts has been established, the $^{206}Pb/^{238}U$ age of 263 ± 2 Ma yielded by zircons separated from the Dashibao basalts, provides an important constraint on Emeishan volcanism. The voluminous basalts of the main Emeishan LIP, along with the Dashibao basalts, rest unconformably on Middle Permian limestone of the Maokou and Sandaoqiao formations, respectively, and relate the Emeishan LIP to the Middle-Late Permian (Guadalupian-Lopingian) boundary (260.4 ± 0.7 Ma, International Stratigraphic Chart, 2008). He and others (2007) dated a clay tuff sample collected from the Middle-Late Permian boundary at Chaotian, Northern Sichuan, and obtained a zircon U-Pb age of 260 ± 4 Ma. On the basis of the geochemical affinity and geochronological consistency, they proposed that the clay bed hosting the dated sample was sourced from Emeishan volcanic activity, and that Emeishan volcanism can be regarded as a boundary event, occurring at ~260 Ma. This is supported by our age for the Dashibao basalt, which is indistinguishable within error from the boundary age, and is also in agreement with the peak age of the intrusions considered to be associated with the LIP (~260 Ma).

This temporal coincidence has prompted many authors to associate the Emeishan LIP with the end-Guadalupian mass extinction (~260 Ma) (Ali and others, 2002; Zhou and others, 2002; Fan and others, 2004; Courtillot and Olson, 2007; Wignall and others, 2009). However, a cause-and-effect scenario can only be true in the case where the volcanism is prior to the extinction. Based on paleomagnetic data and conodont stratigraphic constraints, Ali and others (2002) predicted that the bulk of the Emeishan volcanism should predate the Middle-Late Permian boundary by at least 1.0 to 1.5 Ma. Also, a recent conodont stratigraphic study on the Maokou Formation suggests that eruption of the Emeishan LIP began from the Middle Capitanian Stage (~263 Ma) of the Guadalupian Epoch (Sun and others, 2010). These two results are in accordance with our geochronological data obtained from the Dashibao basalts. However, considering the error on the SHRIMP U-Pb data, a further comprehensive investigation, including more precise dating of the flood basalts, is required to accurately constrain the onset and duration of basalt magmatism in order to substantiate the above hypothesis.

ACKNOWLEDGMENTS

Thanks to Tan Kaixuan and Li Xiaoming for field assistance, and to Jason R. Ali, Guest Editor Simon A. Wilde and an anonymous referee for comprehensive reviews and constructive suggestions that greatly improved the manuscript. This study was financially supported by projects from the Natural Science Foundation of China (40830319, 40825009 and 40721063), the National Basic Research Program of China (2007CB411403) and the Chinese Academy of Sciences (KZCX1-YW-15-5 and KZCX2-YW-128). This is a contribution No. IS-1220 from the Guangzhou Institute of Geochemistry, Chinese Academy of Sciences. This paper is dedicated to Alfred Kröner on the occasion of his 70th birthday.

References

Ali, J. R., Thompson, G. M., Song, X., and Wang, Y., 2002, Emeishan Basalts (SW China) and the "end-Guadalupian" crisis: magnetobiostratigraphic constraints: Journal of the Geological Society, London, v. 159, p. 21–29, doi: 10.1144/0016-764901086.

Ali, J. R., Lo, C.-h., Thompson, G. M., and Song, X., 2004, Emeishan Basalt Ar-Ar overprint ages define several tectonic events that affected the western Yangtze platform in the Mesozoic and Cenozoic: Journal of Asian Earth Sciences, v. 23, p. 163–178, doi: 10.1016/S1367-9120(03)00072-5.

Ali, J. R., Thompson, G. M., Zhou, M.-F., and Song, X., 2005, Emeishan large igneous province, SW China: Lithos, v. 79, p. 475–489, doi: 10.1016/j.lithos.2004.09.013.

Arndt, N. T., Czamanske, G. K., Wooden, J. L., and Fedorenko, V. A., 1993, Mantle and crustal contributions to continental flood volcanism: Tectonophysics, v. 223, p. 39–52, doi: 10.1016/0040-1951(93)90156-E.

Black, L. P., Kamo, S. L., Allen, C. M., Aleinikoff, J. N., Davis, D. W., Korsch, R. J., and Foudoulis, C., 2003, TEMORA 1: a new zircon standard for Phanerozoic U-Pb geochronology: Chemical Geology, v. 200, p. 155–170, doi: 10.1016/S0009-2541(03)00165-7.

Bodinier, J. I., Merlet, C., Bedini, R. M., Simien, F., Remaidi, M., and Garrido, C. J., 1996, Distribution of niobium, tantalum, and other highly incompatible trace elements in the lithospheric mantle: The spinel paradox: Geochimica et Cosmochimica Acta, v. 60, p. 545–550, doi: 10.1016/0016-7037(95)00431-9.

Boven, A., Pasteels, P., Punzalan, L. E., Liu, J., Luo, X., Zhang, W., Guo, Z., and Hertogen, J., 2002, $^{40}Ar/^{39}Ar$ geochronological constraints on the age and evolution of the Permo-Triassic Emeishan Volcanic Province, Southwest China: Journal of Asian Earth Sciences, v. 20, p. 157–175, doi: 10.1016/S1367-9120(01)00031-1.

Burchfiel, B. C., Chen, Z., Liu, Y., and Royden, L. H., 1995, Tectonics of the Longmen Shan and adjacent regions, central China: International Geology Review, v. 37, p. 661–736, doi: 10.1080/00206819509465424.

Chang, E. Z., 2000, Geology and Tectonics of the Songpan-Ganzi Fold Belt, Southwestern China: International Geology Review, v. 42, p. 813–831, doi: 10.1080/00206810009465113.

Chen, C.-Y., and Frey, F. A., 1983, Origin of Hawaiian tholeiite and alkalic basalt: Nature, v. 302, p. 785–789, doi: 10.1038/302785a0.

Chen, S. F., and Wilson, C. J. L., 1996, Emplacement of the Longmen Shan Thrust—Nappe Belt along the eastern margin of the Tibetan Plateau: Journal of Structural Geology, v. 18, p. 413–430, doi: 10.1016/0191-8141(95)00096-V.

Chung, S.-L., and Jahn, B.-m., 1995, Plume-lithosphere interaction in generation of the Emeishan flood basalts at the Permian-Triassic boundary: Geology, v. 23, p. 889–892, doi: 10.1130/0091-7613(1995)023<0889:PLIIGO>2.3.CO;2.

Chung, S. L., Jahn, B. M., Lo, C. H., and Cong, B., 1998, The Emeishan flood basalt in SW China: a mantle plume initiation model and its connection with continental breakup and mass extinction at the Permian-Triassic boundary, *in* Flower, M. F. J., Chung, S. L., Lo, C. H., and Lee, T. L., editors, Mantle dynamics and plate interactions in East Asia: Geodynamics Series: Washington D. C., American Geophysical Union, Geodynamics Series, v. 27, p. 47–58.

Compston, W., Williams, I. S., and Meyer, C., 1984, U-Pb geochronology of zircons form lunar Breccia 73217 using a sensitive high mass-resolution ion microprobe: Journal of Geophysical Research, v. B89, p. 525–534, doi: 10.1029/JB089iS02p0B525.

Courtillot, V., and Olson, P., 2007, Mantle plumes link magnetic superchrons to phanerozoic mass depletion events: Earth and Planetary Science Letters, v. 260, p. 495–504, doi: 10.1016/j.epsl.2007.06.003.

DePaolo, D. J., 1981, Trace element and isotopic effects of combined wallrock assimilation and fractional crystallization: Earth and Planetary Science Letters, v. 53, p. 189–202, doi: 10.1016/0012-821X(81)90153-9.

Fan, W.-M., Wang, Y.-J., Peng, T.-P., Miao, L.-C., and Guo, F., 2004, Ar-Ar and U-Pb geochronology of Late Paleozoic basalts in western Guangxi and its constraints on the eruption age of Emeishan basalt magmatism: Chinese Science Bulletin, v. 49, p. 2318–2327, doi: 10.1360/04wd0201.

Fan, W., Zhang, C., Wang, Y., Guo, F., and Peng, T., 2008, Geochronology and geochemistry of Permian basalts in western Guangxi Province, Southwest China: Evidence for plume-lithosphere interaction: Lithos, v. 102, p. 218–236, doi: 10.1016/j.lithos.2007.09.019.

Frey, F. A., Garcia, M. O., and Roden, M. F., 1994, Geochemical characteristics of Koolau Volcano: Implications of intershield geochemical differences among Hawaiian volcanoes: Geochimica et Cosmochimica Acta, v. 58, p. 1441–1462, doi: 10.1016/0016-7037(94)90548-7.

Gaherty, J. B., 2001, Seismic Evidence for Hotspot-Induced Buoyant Flow Beneath the Reykjanes Ridge: Science, v. 293, p. 1645–1647, doi: 10.1126/science.1061565.

Gallagher, K., and Hawkesworth, C., 1992, Dehydration melting and the generation of continental flood basalts: Nature, v. 358, p. 57–59, doi: 10.1038/358057a0.

Garland, F., Turner, S., and Hawkesworth, C., 1996, Shifts in the source of the Paraná basalts through time: Lithos, v. 37, p. 223–243, doi: 10.1016/0024-4937(95)00038-0.

Griffiths, R. W., and Campbell, I. H., 1990, Stirring and structure in mantle starting plumes: Earth and Planetary Science Letters, v. 99, p. 66–78, doi: 10.1016/0012-821X(90)90071-5.

Guo, F., Fan, W. M., Wang, Y. J., and Li, C. W., 2004, When did the Emeishan mantle plume activity start? Geochronological and geochemical evidence from ultramafic-mafic dikes in southwestern China: International Geology Review, v. 46, p. 226–234, doi: 10.2747/0020-6814.46.3.226.

He, B., Xu, Y.-G., Chung, S.-L., Xiao, L., and Wang, Y., 2003, Sedimentary evidence for a rapid, kilometer-scale crustal doming prior to the eruption of the Emeishan flood basalts: Earth and Planetary Science Letters, v. 213, p. 391–405, doi: 10.1016/S0012-821X(03)00323-6.

He, B., Xu, Y.-G., Wang, Y.-M., and Luo, Z.-Y., 2006, Sedimentation and Lithofacies Paleogeography in Southwestern China Before and After the Emeishan Flood Volcanism: New Insights into Surface Response to Mantle Plume Activity: The Journal of Geology, v. 114, p. 117–132, doi: 10.1086/498103.

He, B., Xu, Y.-G., Huang, X.-L., Luo, Z.-Y., Shi, Y.-R., Yang, Q.-J., and Yu, S.-Y., 2007, Age and duration of the Emeishan flood volcanism, SW China: Geochemistry and SHRIMP zircon U-Pb dating of silicic ignimbrites, post-volcanic Xuanwei Formation and clay tuff at the Chaotian section: Earth and Planetary Science Letters, v. 255, p. 306–323, doi: 10.1016/j.epsl.2006.12.021.

Hollanda, M. H. B. M., Pimentel, M. M., Oliveira, D. C., and de Sa, E. F. J., 2006, Lithosphere-asthenosphere interaction and the origin of Cretaceous tholeiitic magmatism in Northeastern Brazil: Sr-Nd-Pb isotopic evidence: Lithos, v. 86, p. 34–49, doi: 10.1016/j.lithos.2005.04.004.

Huang, K., and Opdyke, N. D., 1998, Magnetostratigraphic investigations on an Emeishan basalt section in western Guizhou province, China: Earth and Planetary Science Letters, v. 163, p. 1–14, doi: 10.1016/S0012-821X(98)00169-1.

Huang, M., Maas, R., Buick, I. S., and Williams, I. S., 2003, Crustal response to continental collisions between the Tibet, Indian, South China and North China Blocks: geochronological constraints from the Songpan-Garzê Orogenic Belt, western China: Journal of Metamorphic Geology, v. 21, p. 223–240, doi: 10.1046/j.1525-1314.2003.00438.x.

ICS, 2008, International Stratigraphic Chart: International Commission on Stratigraphy.

Johnson, K. T. M., Dick, H. J. B., and Shimizu, N., 1990, Melting in the oceanic upper mantle: an ion microprobe study of diopsides in abyssal peridotites: Journal of Geophysical Research, v. 95, p. 2661–2678, doi: 10.1029/JB095iB03p02661.

Kinzler, R. J., 1997, Melting of mantle peridotite at pressures approaching the spinel to garnet transition: Application to mid-ocean ridge basalt petrogenesis: Journal of Geophysical Research, v. 102, p. 853–874, doi: 10.1029/96JB00988.

Lassiter, J. C., and DePaolo, D. J., 1997, Plume/lithosphere interaction in the generation of continental and oceanic flood basalts: chemical and isotope constraints, *in* Mahoney, J., and Coffin, M. F., editors, Large Igneous Provinces: Continental, Oceanic, and Planetary Flood Volcanism: American Geophysical Union, Geophyscial Monograph Series, v. 100, p. 335–355.

Liang, X. R., Wei, G. J., Li, X. H., and Liu, Y., 2003, Precise measurement of $^{143}Nd/^{144}Nd$ and Sm/Nd ratios using multiple-collectors inductively coupled plasma-mass spectrometer (MC-ICPMS): Geochimica, v. 32, p. 91–96 (in Chinese with English abstract).

Lightfoot, P. C., Hawkesworth, C. J., Hergt, J., Naldrett, A. J., Gorbachev, N. S., Fedorenko, V. A., and Doherty, W., 1993, Remobilisation of the continental lithosphere by a mantle plume: major-, trace-element, and Sr-, Nd-, and Pb-isotope evidence from picritic and tholeiitic lavas of the Noril'sk District, Siberian Trap, Russia: Contributions to Mineralogy and Petrology, v. 114, p. 171–188, doi: 10.1007/BF00307754.

Lo, C.-H., Chung, S.-L., Lee, T.-Y., and Wu, G., 2002, Age of the Emeishan flood magmatism and relations to Permian-Triassic boundary events: Earth and Planetary Science Letters, v. 198, p. 449–458, doi: 10.1016/S0012-821X(02)00535-6.

Ludwig, K. R., 2001a, Squid 1.02: A user manual: Berkeley Geochronological Center Special Publication, p. 19.

——— 2001b, User's Manual for Isoplot/Ex rev.2.49: A Geochronological Toolkit for Microsoft Excel: Berkeley Geochronology Centre Special Publication, v. 1a, p. 55.

Macdonald, G. A., and Katsura, T., 1964, Chemical Composition of Hawaiian Lavas: Journal of Petrology, v. 5, p. 82–133, doi: 10.1093/petrology/5.1.82.

McKenzie, D., and O'Nions, R. K., 1991, Partial Melt Distributions from Inversion of Rare Earth Element Concentrations: Journal of Petrology, v. 32, p. 1021–1091, doi: 10.1093/petrology/32.5.1021.

Meschede, M., 1986, A method of discriminating between different types of mid-ocean ridge basalts and continental tholeiites with the Nb-Zr-Y diagram: Chemical Geology, v. 56, p. 207–218, doi: 10.1016/0009-2541(86)90004-5.

Montagner, J.-P., and Ritsema, J., 2001, Interactions Between Ridges and Plumes: Science, v. 294, p. 1472–1473, doi: 10.1126/science.1067486.

Noll, P. D., Jr., Newsom, H. E., Leeman, W. P., and Ryan, J. G., 1996, The role of hydrothermal fluids in the production of subduction zone magmas: Evidence from siderophile and chalcophile trace elements and boron: Geochimica et Cosmochimica Acta, v. 60, p. 587–611, doi: 10.1016/0016-7037(95)00405-X.

Pearce, J. A., 1983, The role of sub-continental lithosphere in magma genesis at destructive plate margins, *in* Hawkesworth, C. J., and Norry, M. J., editors, Continental Basalts and Mantle Xenoliths: Nantwich, Shiva, p. 230–249.

Pearce, J. A., and Cann, J. R., 1973, Tectonic setting of basic volcanic rocks determined using trace element analyses: Earth and Planetary Science Letters, v. 19, p. 290–300, doi: 10.1016/0012-821X(73)90129-5.

Peate, I. U., and Bryan, S. E., 2008, Re-evaluating plume-induced uplift in the Emeishan large igneous province: Nature Geoscience, v. 1, p. 625–629, doi: 10.1038/ngeo281.

Qi, L., Hu, J., and Gregoire, D. C., 2000, Determination of trace elements in granites by inductively coupled plasma mass spectrometry: Talanta, v. 51, p. 507–513, doi: 10.1016/S0039-9140(99)00318-5.

SBGMR (Sichuan Bureau of Geology and Mineral Resources), 1976, Sichuan Geological Map Series: Baoxing Sheet (H-48-13), scale 1:200,000 (in Chinese).

——— 1983, Sichuan Geological Map Series: Xiaojin Sheet (H-48-07) scale 1:200,000 (in Chinese).

——— 1991, Regional Geology of Sichuan Province: Beijing, Geological Publishing House (in Chinese).

——— 1997, Stratigraphy (lithostratic) of Sichuan Province: Wuhan, China University of Geosciences Press, 417 p (in Chinese).

Shellnutt, J. G., and Zhou, M.-F., 2007, Permian peralkaline, peraluminous and metaluminous A-type granites in the Panxi district, SW China: Their relationship to the Emeishan mantle plume: Chemical Geology, v. 243, p. 286–316, doi: 10.1016/j.chemgeo.2007.05.022.

——— 2008, Permian, rifting related fayalite syenite in the Panxi region, SW China: Lithos, v. 101, p. 54–73, doi: 10.1016/j.lithos.2007.07.007.

Song, B., Zhang, Y. H., Wan, Y. S., and Jian, P., 2002, Mount making and procedure of the SHRIMP dating: Geological Review, v. 48, p. 26–30 (in Chinese with English abstract).

Song, X., Hou, Z. Q., Cao, Z., Lu, J., Wang, Y., Zhang, C., and Li, Y., 2001, Geochemical characteristics and period of the Emei Igneous Province: Acta Geologica Sinica, v. 75, p. 498–506.

Song, X.-Y., Zhou, M.-F., Cao, Z.-M., and Robinson, P. T., 2004, Late Permian rifting of the South China Craton caused by the Emeishan mantle plume?: Journal of the Geological Society, London, v. 161, p. 773–781, doi: 10.1144/0016-764903-135.

Song, X.-Y., Zhou, M.-F., Keays, R. R., Cao, Z.-M., Sun, M., and Qi, L., 2006, Geochemistry of the Emeishan flood basalts at Yangliuping, Sichuan, SW China: implications for sulfide segregation: Contributions to Mineralogy and Petrology, v. 152, p. 53–74, DOI: 10.1007/s00410-006-0094-3.

Song, X.-Y., Qi, H.-W., Robinson, P. T., Zhou, M.-F., Cao, Z.-M., and Chen, L.-M., 2008, Melting of the subcontinental lithospheric mantle by the Emeishan mantle plume; evidence from the basal alkaline basalts in Dongchuan, Yunnan, Southwestern China: Lithos, v. 100, p. 93–111, doi: 10.1016/j.lithos.2007.06.023.

Sun, S. s., and McDonough, W. F., 1989, Chemical and isotopic systematics of oceanic basalts: implications for mantle composition and processes, *in* Saunders, A. D., and Norry, M. J., editors, Magmatism in the Ocean Basins: Geological Society of London, Special Publication, v. 42, p. 313–345, doi: 10.1144/GSL.SP.1989.042.01.19.

Sun, Y., Lai, X., Wignall, P. B., Widdowson, M., Ali, J. R., Jiang, H., Wang, W., Yan, C., Bond, D. P. G., and Védrine, S., 2010, Dating the onset and nature of the Middle Permian Emeishan large igneous province eruptions in SW China using conodont biostratigraphy and its bearing on mantle plume uplift models: Lithos, v. 119, p. 20–33, doi: 10.1016/j.lithos.2010.05.012.

Taylor, S. R., and McLennan, S. M., 1985, The continental crust: Its composition and evolution: Oxford, United Kingdom, Blackwell, 312 p.

Walter, M. J., 1998, Melting of garnet peridotite and the origin of komatiite and depleted lithosphere: Journal of Petrology, v. 39, p. 29–60, doi: 10.1093/petroj/39.1.29.

Wignall, P. B., Sun, Y., Bond, D. P. G., Izon, G., Newton, R. J., Védrine, S., Widdowson, M., Ali, J. R., Lai, X., Jiang, H., Cope, H., and Bottrell, S. H., 2009, Volcanism, Mass Extinction, and Carbon Isotope Fluctuations in the Middle Permian of China: Science, v. 324, p. 1179–1182, doi: 10.1126/science.1171956.

Williams, I. S., 1998, U-Th-Pb geochronology by ion microprobe, *in* McKibben, M. A., Shanks, W. C., III., and Ridley, W. I., editors, Applications of microanalytical techniques to understanding mineralizing processes: Reviews in Economic Geology, v. 7, p. 1–35.

Winchester, J. A., and Floyd, P. A., 1977, Geochemical discrimination of different magma series and their differentiation products using immobile elements: Chemical Geology, v. 20, p. 325–343, doi: 10.1016/0009-2541(77)90057-2.

Wooden, J. L., Czamanske, G. K., Fedorenko, V. A., Arndt, N. T., Chauvel, C., Bouse, R. M., King, B.-S. W., Knight, R. J., and Siems, D. F., 1993, Isotopic and trace-element constraints on mantle and crustal contributions to Siberian continental flood basalts, Noril'sk area, Siberia: Geochimica et Cosmochimica Acta, v. 57, p. 3677–3704, doi: 10.1016/0016-7037(93)90149-Q.

Xiao, L., and Xu, J., 2005, Petrogenesis and tectonic setting of Dashibao Group basalts from Songpan-Ganze block, northwestern Sichuan province, China: Acta Petrologica Sinica, v. 21, p. 1539–1545 (in Chinese with English abstract).

Xiao, L., Xu, Y. G., Mei, H. J., Zheng, Y. F., He, B., and Pirajno, F., 2004, Distinct mantle sources of low-Ti and high-Ti basalts from the western Emeishan large igneous province, SW China: implications for plume-lithosphere interaction: Earth and Planetary Science Letters, v. 228, p. 525–546, doi: 10.1016/j.epsl.2004.10.002.

Xu, Y., Chung, S.-L., Jahn, B.-m., and Wu, G., 2001, Petrologic and geochemical constraints on the petrogenesis of Permian-Triassic Emeishan flood basalts in southwestern China: Lithos, v. 58, p. 145–168, doi: 10.1016/S0024-4937(01)00055-X.

Xu, Y.-G., and He, B., 2007, Thick, high-velocity crust in the Emeishan large igneous province, southwestern China: Evidence for crustal growth by magmatic underplating or intraplating, *in* Foulger, G. R., and Jurdy, D. M., editors, Plates, plumes, and planetary processes: Geological Society of America Special Papers, v. 430, p. 841–858, doi: 10.1130/2007.2430(39).

Xu, Y.-G., He, B., Chung, S.-L., Menzies, M. A., and Frey, F. A., 2004, Geologic, geochemical, and geophysical consequences of plume involvement in the Emeishan flood-basalt province: Geology, v. 32, p. 917–920, doi: 10.1130/G20602.1.

Xu, Y.-G., Luo, Z.-Y., Huang, X.-L., He, B., Xiao, L., Xie, L.-W., and Shi, Y.-R., 2008, Zircon U-Pb and Hf isotope constraints on crustal melting associated with the Emeishan mantle plume: Geochimica et Cosmochimica Acta, v. 72, p. 3084–3104, doi: 10.1016/j.gca.2008.04.019.

Yin, A., and Harrison, T. M., 2000, Geologic Evolution of the Himalayan-Tibetan Orogen: Annual Review of Earth and Planetary Sciences, v. 28, p. 211–280, doi: 10.1146/annurev.earth.28.1.211.

Zhang, Z. C., and Wang, F. S., 2002, Geochemistry of two types of basalts of the Emeishan basaltic Province: Evidence for mantle plume-lithosphere interaction: Acta Geologica Sinica, v. 76, p. 229–237, doi: 10.1111/j.1755-6724.2002.tb00088.x.

Zhang, Z., Mahoney, J. J., Mao, J., and Wang, F., 2006, Geochemistry of Picritic and Associated Basalt Flows of the Western Emeishan Flood Basalt Province, China: Journal of Petrology, v. 47, p. 1997–2019, doi: 10.1093/petrology/egl034.

Zhong, H., Zhu, W.-G., Chu, Z.-Y., He, D.-F., and Song, X.-Y., 2007, Shrimp U-Pb zircon geochronology, geochemistry, and Nd-Sr isotopic study of contrasting granites in the Emeishan large igneous province, SW China: Chemical Geology, v. 236, p. 112–133, doi: 10.1016/j.chemgeo.2006.09.004.

Zhou, M.-F., Malpas, J., Song, X.-Y., Robinson, P. T., Sun, M., Kennedy, A. K., Lesher, C. M., and Keays, R. R., 2002, A temporal link between the Emeishan large igneous province (SW China) and the end-Guadalupian mass extinction: Earth and Planetary Science Letters, v. 196, p. 113–122, doi: 10.1016/S0012-821X(01)00608-2.

Zhou, M.-F., Robinson, P. T., Lesher, C. M., Keays, R. R., Zhang, C.-J., and Malpas, J., 2005, Geochemistry, Petrogenesis and Metallogenesis of the Panzhihua Gabbroic Layered Intrusion and Associated Fe-Ti-V Oxide Deposits, Sichuan Province, SW China: Journal of Petrology, v. 46, p. 2253–2280, doi: 10.1093/petrology/egi054.

Zhou, M.-F., Zhao, J.-H., Qi, L., Su, W., and Hu, R., 2006, Zircon U-Pb geochronology and elemental and Sr-Nd isotope geochemistry of Permian mafic rocks in the Funing area, SW China: Contributions to Mineralogy and Petrology, v. 151, p. 1–19, doi: 10.1007/s00410-005-0030-y.

Zhou, M.-F., Arndt, N. T., Malpas, J., Wang, C. Y., and Kennedy, A. K., 2008, Two magma series and associated ore deposit types in the Permian Emeishan large igneous province, SW China: Lithos, v. 103, p. 352–368, doi: 10.1016/j.lithos.2007.10.006.

Zi, J.-W., Fan, W.-M., Wang, Y.-J., and Peng, T.-P., 2008a, Geochemistry of Dashibao Formation high-Ti basalts from Baoxing in Sichuan Province, Southwest China and their petrogenesis: Geochemica, v. 37, p. 9–21 (in Chinese with English abstract).

Zi, J., Fan, W., Wang, Y., Peng, T., and Guo, F., 2008b, Geochemistry and petrogenesis of the Permian mafic dykes in the Panxi region, SW China: Gondwana Research, v. 14, p. 368–382, doi: 10.1016/j.gr.2008.02.008.